mini-MEndR: A 96-well mixed species culture assay to co-evaluate human and mouse Pax7^{+} cell-mediated skeletal muscle repair

Nitya Gulati[1,2†], Sadegh Davoudi[2,3†], Bin Xu[2,3†], Saifedine T. Rjaibi[1-3‡], Erik Jacques[2,3‡], Justin Pham[1,2], Amir Fard[1-3], Alison P. McGuigan[1,3*], Penney M. Gilbert[2-4*]

[1] Department of Chemical Engineering and Applied Chemistry, University of Toronto, Toronto, ON, M5S3E4, Canada

[2] Donnelly Centre, University of Toronto, Toronto, ON M5S3E1, Canada

[3] Institute of Biomedical Engineering, University of Toronto, Toronto, ON, M5S3G9, Canada

[4] Department of Cell and Systems Biology, University of Toronto, Toronto, ON M5S3G5, Canada

[*] Co-corresponding author e-mails: penney.gilbert@utoronto.ca (P.M.G.) and alison.mcguigan@utoronto.ca (A.P.M.)

[†] These authors contributed equally to this work.

[‡] These authors contributed equally to this work.

Abstract

Functional evaluation of molecules that are predicted to promote stem cell mediated endogenous repair often requires *in vivo* transplant studies that are low throughput and hinder the rate of discovery. Here, we offer a strategy to rapidly test and prioritize molecules for functional validation studies. We miniaturized, simplified and expanded the functionality of a previously developed muscle endogenous repair (MEndR) *in vitro* assay that was shown to capture significant events of the first week of the *in vivo* muscle endogenous repair process. The new "mini-MEndR assay" consists of miniaturized cellulose scaffolds designed to fit in 96-well plates. The scaffold pores are infiltrated with myoblasts encapsulated in a fibrin-based hydrogel to form thin, engineered skeletal muscle tissues. By evaluating multiple commercially available human primary myoblast lines in 2D and 3D culture, we establish quality assurance metrics for cell line selection that standardize myotube template quality. Pre-adsorbing thrombin to the cellulose scaffolds facilitates *in situ* tissue polymerization, a critical modification that enables users proficient in myoblast culture to rapidly acquire myotube template fabrication expertise. Following the generation of the 3D myotube template, muscle stem cells (MuSCs), enriched from digested mouse skeletal muscle tissue using an improved magnetic-activated cell sorting protocol, are engrafted onto the engineered human muscle template. A regenerative milieu is then introduced by injuring the muscle tissue with a myotoxin. Addition of a known modulator of MuSC mediated repair recapitulates the *in vivo* outcomes (enhanced muscle production and $Pax7^+$ cell expansion), but only in the presence of both the stem cells and the regenerative milieu. By fluorescently labeling the mouse MuSCs, we demonstrate the feasibility of co-evaluating human and mouse $Pax7^+$ cell responses to drug treatment, thereby expanding the utility of the assay. Importantly, phenotypic data is collected with a high-content imaging system and is analyzed using CellProfiler-based image analysis pipelines. The miniaturized predictive assay offers a simple, scaled platform with which to co-investigate human and mouse skeletal muscle endogenous repair molecular modulators, and thus is a promising strategy to accelerate the muscle endogenous repair discovery pipeline.

Key Words: predictive assay, scale-up, manufacturing, skeletal muscle, stem cell, endogenous repair

62 **Introduction**

63 The regenerative capacity of healthy skeletal muscle is driven by the activity of tissue resident
64 muscle stem cells (MuSCs). With age[1], or in disease, e.g. Duchenne muscular dystrophy (DMD)[2,3],
65 MuSCs remain present, but have diminished repair capabilities. Therapeutic strategies to correct
66 diminished skeletal muscle endogenous repair have a growing need. One exciting emerging
67 strategy to improve skeletal muscle endogenous repair is the use of drugs to boost MuSC function
68 (i.e. endogenous repair), for which pre-clinical studies in mice demonstrate the promise of this
69 therapeutic approach[3–6].

70 A current gold standard assay to determine whether a molecular target restores MuSC
71 function, and thus to make a go/no-go decision in the discovery process, is the intramuscular
72 transplantation assay[7–9]. This assay involves transplanting treated cells into the pre-irradiated and
73 pre-injured hindlimb of immune-compromised rodents and then assessing the capacity of the
74 transplanted cell population to make muscle and repopulate the stem cell compartment. This gold-
75 standard assay is expensive, low throughput and plagued by high variation, which in turn limits
76 the number of candidates that can be tested. To overcome this pain point in the discovery process,
77 we[10] and others[11,12], have invented in vitro functional assays to predict skeletal muscle endogenous
78 repair outcomes "in a dish" as a lower cost complement to the intramuscular transplantation assay.
79 Most of the assays evaluate engineered skeletal muscle microtissue repair after an induced injury.
80 Since the primary myoblast cultures used to produce the microtissues contain Pax7^{+} cells, tissue
81 repair is attributed to the activity of this sub-population. By contrast, the muscle endogenous repair
82 (MEndR) assay tracks the activity of bonefide MuSCs engrafted into thin engineered muscle
83 tissues that are suited to long-term timelapse microscopy[10].

84 In the MEndR culture assay, we first engineer thin sheets of mature skeletal muscle tissue
85 by infiltrating a thin cellulose (paper) scaffold with primary patient-derived muscle progenitor
86 cells encapsulated in an extracellular matrix hydrogel. MuSCs freshly isolated from mouse
87 hindlimb skeletal muscle tissue are labelled and then incorporated into the 3D muscle sheets.
88 Shortly thereafter, the muscle tissue sheet is injured by exposure to a myotoxin to induce a
89 regenerative microenvironment, and MuSC-mediated muscle tissue template repair is assessed
90 phenotypically by assessing the contribution of labelled MuSCs to new muscle tissue formation,
91 and to niche repopulation, using fluorescent image analysis. To validate the predictability of our
92 platform, we tested a number of drugs that were previously reported modulators of MuSC function

93 and compared results using MEndR with those we obtained in parallel using the *in vivo*
94 transplantation assay. MEndR accurately predicted *in vivo* transplantation assay outcomes. Side-
95 by-side comparisons accurately identified a range of repair phenotypes observed in the *in vivo*
96 transplantation assay results. Furthermore, since MEndR tissues are thin and flat, the user has
97 greater control over the conditions during drug testing than with the previously described
98 microtissue based assays[11,12] (e.g., MuSC content, state of the template, uniform exposure to media
99 components). With this prior study[10], we demonstrated for the first time, the ability to compress
100 the translational pipeline by offering a complement to the *in vivo* validation assay that is, in theory,
101 amenable to testing all 2D drug screen 'hits' without the need for biased pre-selection.
102 The MEndR functional assay is poised to serve as a secondary screen service to prioritize
103 'hits' arising from high-throughput screens designed to discover MuSC potency modulators.
104 However, MEndR assay scale-up from a 24-well footprint to a 96-well format is critical to realizing
105 this goal. Candidate assessment performed in a 96-well format has the potential to offer an order
106 of magnitude higher throughput than the intramuscular transplantation assay. Towards this goal,
107 we herein describe the scaling of the MEndR assay into a 96-well footprint and we validate that
108 the miniaturized platform captures all stem cell functional metrics shown in the original MEndR
109 platform. We also extend the utility of the assay by demonstrating the capacity to co-evaluate
110 responses of human (within myotube template) and mouse (engrafted MuSCs) $Pax7^{+}$ populations
111 to molecule treatments.
112
113 **Materials and Methods**
114 **Human myoblast maintenance and 2D differentiation**
115 Human primary myoblasts (pMB) were purchased from Cook MyoSite® (Table 1). For routine
116 culture, myoblasts were plated on collagen-coated tissue culture plates (Table 2) at a seeding
117 density of 5000 - 7500 cells/cm^2. Myoblasts were maintained in human pMB growth medium
118 (GM; Table 2) and passaged using trypsin upon reaching ~70% confluency. Culture media was
119 replaced every other day. Myoblasts were used at passage 6-7 for 2D experiments, and at passage
120 8 in all 3D tissue experiments. For 2D differentiation studies, myoblasts were plated at a seeding
121 density of ~37,000 cells/cm^2 on Geltrex™ coated plates in human pMB GM. The cultures were
122 transitioned to 2D differentiation media (DM; Table 2) one-day post seeding to induce fusion. Half

123 of the DM was removed and replaced every other day. Cultures were fixed and analyzed on day 9
124 of differentiation.
125
126 **MEndR and mini-MEndR myotube template fabrication and injury**
127 24-well plate format myotube templates were generated as previously described by our group[10].
128 Briefly, rectangle patterns with 0.5 cm x 1 cm dimensions were printed onto the cellulose scaffold
129 product (MiniMinit® Products Ltd) with a LaserJet printer and then cut into individual rectangular
130 scaffolds with scissors. These scaffolds were then autoclaved in a dry cycle to maintain sterility.
131 To generate the myotube templates, sterile cellulose scaffolds were carefully placed on a custom
132 polydimethylsiloxane (PDMS) block using a pair of sterile tweezers. The PDMS block was placed
133 in an ethanol-sterilized plastic container with moist paper on the bottom and a tight-fitting lid to
134 seal the top, to create a humidified chamber. Next, a fibrinogen solution (Table 2) was freshly
135 prepared and filter-sterilized with a 0.22 µm filter. pMBs were resuspended at a concentration of
136 (3.33E+07 cells/mL) in an extracellular matrix (ECM) master mix (Table 2). 100 U/mL of
137 thrombin (Sigma, #T6884) was added to the pMB/ECM mixture to achieve a final concentration
138 of 0.225 U/mg of fibrinogen. The mixture was maintained on ice throughout. Next, 12 µL of
139 pMB/ECM mixture (i.e., 4.0E+05 pMBs) was evenly distributed onto the cellulose scaffolds using
140 a custom spreading tool[13]. The humidified chamber was then sealed with the lid and incubated at
141 37 °C for 5 minutes to encourage conversion of fibrinogen to fibrin clots. Next, MEndR GM (Table
142 2) was gently pipetted onto each of the scaffolds to facilitate easy detachment from the PDMS
143 block. The scaffolds were then gently lifted and placed into individual wells of a 24-well plate
144 containing 1 mL of MEndR GM. Two days later, the GM was removed and replaced with MEndR
145 DM to facilitate myotube differentiation. Half of the MEndR DM was removed and replaced every
146 other day.
147 For 96-well plate format myotube templates (mini-myotube templates), cellulose paper
148 (MiniMinit® Products Ltd) was cut into circular discs using a 5 mm biopsy punch (Integra,
149 #MLT3335) and subsequently sterilized in an autoclave. 96-well plates (PhenoPlate 96-well
150 microplates, PerkinElmer) were prepared for tissue seeding and culture by treatment with 100 µl
151 of 5 % Pluronic F-127 (Sigma, Cat#P2443) solution in dH_2O (Table 2) at 4 °C overnight, or
152 minimum one hour, which served to create a non-adhesive surface to prevent cell attachment on
153 the plates and facilitate tissue self-organization. The pluronic acid was then aspirated, and the plate

154 was left to dry in the biosafety cabinet with the lid removed until the thin film of liquid could no
155 longer be visualized (~20 min). The autoclaved disks were then placed in the center of the
156 corresponding wells of the 96-well plate using a sterile anti-static tweezer. Next, a 0.8 U/mL
157 thrombin solution was prepared by diluting the 100 U/mL thrombin stock in PBS, and 4 µL of the
158 0.8 U/mL thrombin solution was dispensed onto the center of each paper disc. The discs were then
159 left to dry in the biosafety cabinet. Meanwhile, a 10 mg/mL fibrinogen solution (Table 2) was
160 freshly prepared by dissolving lyophilized fibrinogen powder in 0.9 % wt./vol of NaCl solution,
161 and subsequently sterilized by passing through a 0.22 µm filter. pMBs were trypsinized, counted
162 and suspended in ECM master mix (Table 2) at a concentration of 2.5E+07 cells/mL, which was
163 kept on ice. Next, 4 µL of pMB/ECM mixture (i.e., 1.0E+05 pMBs) was pipetted into the center
164 of paper discs with pre-adsorbed thrombin, with the mixture entering the cellulose scaffold pores
165 by capillary action. Cellulose scaffolds impregnated with pMB/ECM were incubated for 5 minutes
166 at 37 °C. 200 µL of MEndR GM (Table 2) was then gently pipetted into each well, ensuring that
167 the tissues did not flip over. The 96-well plate was then returned to the cell culture incubator (37
168 °C, 5 % CO_2). The next day, tissues that failed to detach from the bottom of the well (by visual
169 inspection), were released by gently triturating the culture media in the well with a p200 pipette.
170 Two days later, the MEndR GM was aspirated and replaced with MEndR DM (Table 2). Half of
171 the MEndR DM was removed and replaced with fresh medium every other day.
172
173 **Immunohistochemistry**
174 2D myotube cultures, and 3D muscle tissues, were harvested and fixed at the indicated culture
175 endpoints by removing the media, washing gently three times with phosphate buffered saline
176 (PBS), and then incubating in 200 µL of 4% paraformaldehyde for 15 min at room temperature.
177 The samples were washed three times with PBS every 5 min followed by incubation in blocking
178 solution (Table 3) overnight at 4 °C, or for 1 hr at room temperature. Following blocking, which
179 also contains permeabilization agent, samples were then incubated with 40 µL of primary
180 antibodies (Table 3) diluted in PBS and 0.1 % goat serum, overnight at 4 °C. Next, the samples
181 were washed three times with cold PBS every 10 min and then incubated for 45-60 min at room
182 temperature with 40 µL of a secondary antibody mix (Table 3), containing DRAQ5 nuclear counter
183 stain (Table 3), and diluted in PBS with 0.1% goat serum. The secondary antibody mix contained
184 phalloidin conjugates (Table 3) for the experiments where phalloidin coverage was assessed. The

185 samples were then washed three times with cold PBS. Tissue samples were stored in PBS at 4 °C
186 until image acquisition.
187
188 **Image acquisition**
189 Confocal z-stack images of immunostained samples were acquired using an Olympus FV-1000
190 confocal microscope and Olympus FluoView V4.2b imaging software. Images were acquired
191 using x4 (0.13 NA), x10 (0.3 NA) or x20 (0.45 NA) air objectives (Olympus) and the step size for
192 each z-stack image acquired was set at the optimal value for each objective by the imaging
193 software. Laser power, PMT HV and background offset were adjusted using the grey scale scan.
194 Laser power was set lower than 75 % during image acquisition to prevent photobleaching and
195 reduce cytotoxicity for all images. Next, laser power and HV were adjusted to avoid overexposure
196 and saturation as guided by the red pixels. Background offset was adjusted to preclude blue pixels
197 in each of the stacks. HV was set lower than 750 to reduce noise and Gain was set at 1 for all
198 images. For the niche repopulation experiments, tissues were imaged using an Opera Phenix High
199 Content Screening system outfitted with a x20 water immersion objective. Confocal stacks were
200 converted to the 2D space using a maximum Z-projection prior to image analysis. Nuclear fusion
201 index, $Pax7^+$ cell enumerations, as well as sarcomeric α-actinin (SAA), green or yellow fluorescent
202 protein (GFP/YFP) or phalloidin tissue coverage were quantified exactly as we previously
203 described[10].
204
205 **Bead retention assay and analysis**
206 Cellulose-based paper scaffolds (MiniMinit® Products Ltd) were cut using a 5 mm diameter
207 biopsy puncher and placed in a 96-well plate. Scaffolds were pre-adsorbed with thrombin at a
208 concentration of 0.8 U/ml (0.2 U/mg fibrinogen) and allowed to dry for one hour in the biological
209 safety cabinet with the 96-well plate lid removed. Next, a Master Mix was prepared by diluting 15
210 µm diameter fluorescent beads (Bangslab, #FCDG011) 10 times in ECM master mix (Table 2).
211 Then, 4 µL of the bead MasterMix was infiltrated into each of the dried scaffolds and the scaffolds
212 were subsequently incubated at 37 °C for 5-10 min to allow the Master Mix and thrombin to gel.
213 The scaffolds were imaged using confocal microscopy (Olympus FV-1000, x4 air
214 objective, laser power 20-40 %, HV < 700) to determine the initial number of beads. Scaffolds
215 were maintained in PBS while not being imaged to prevent them from drying. After the initial

216 images were captured, scaffolds were washed with PBS three times to mimic the turbulence
217 experienced by scaffolds during 3D culture (e.g., media changes). The scaffolds were imaged once
218 more, using the same settings, to determine the number of beads retained.
219 To quantify the number of beads in an image, confocal stacks were first converted to the
220 2D space using a maximum Z-projection. Thresholding was performed using FIJI's built-in Yen
221 algorithm to binarize the image into fluorescent beads and background. Overlapping adjacent
222 beads were segmented using the watershed tool. Finally, FIJI's *Analyze Particles* function was
223 used to count the number of beads recorded in the image.
224
225 **Mini-myotube template endogenous repair**
226 To study myotube template endogenous repair potential, we optimized an injury protocol that
227 achieved an ~50 % reduction in SAA coverage of the myotube template post injury. Specifically,
228 the culture media was removed from the myotube template tissues and replaced with MEndR DM
229 containing 0.5 μM cardiotoxin (CTX) (Latoxan #L8102 – diluted in water) on day 7 of
230 differentiation. Tissues were incubated on an orbital shaker in a 37 °C incubator for 4 hours. The
231 medium was gently pipetted at the 2-hour mark to encourage the movement of the medium in the
232 well and the detachment of any broken fibers. After the 4-hour incubation, cardiotoxin was
233 removed by gently washing the tissues twice with MEndR DM. Tissues were then cultured in
234 MEndR DM supplemented with 5 ng/mL rh-FGF2 for 24 hr, to assess template injury.
235 For myotube template self-repair studies, tissues were first cultured for a period of 5 days
236 post injury, during which time the tissues were treated with endogenous repair stimulating drugs
237 as indicated in Table 4. The MEndR DM supplemented with FGF2 and drugs was completely
238 replaced every other day. For the remaining duration of the assay, tissues were cultured in MEndR
239 DM and half of the media was replaced every other day.
240
241 **Mouse strains and ethics**
242 All animal use protocols were reviewed and approved by the local Animal Care Committee (ACC)
243 within the Division of Comparative Medicine (DCM) at the University of Toronto. All methods in
244 this study were conducted as described in the approved animal use protocols (#20012838) and
245 more broadly in accordance with the guidelines and regulations of the DCM ACC and the
246 Canadian Council on Animal Care. 129-Tg(CAG-EYFP)/7AC5Nagy/J mice are maintained by

247 crossing homozygous males and females. C57BL/6-Tg (CAG-EGFP)1Osb/J (Actin-eGFP) mice
248 were purchased from the Jackson Laboratory (USA) and utilized in experiments after a 1-week
249 acclimatization period. Tg(Pax7-nGFP) mice[14] were a kind gift from Dr. Shahragim Tajbakhsh,
250 transferred from the laboratory of Dr. Michael Rudnicki and maintained at the University of
251 Toronto by backcrossing to C57Bl/10ScSn (Jackson Laboratory) and genotyping for the GFP gene.
252 For all experiments, 8-12 week old female mice were used.
253
254 **Murine muscle stem cell (MuSC) isolation**
255 MuSCs were prospectively isolated from the collective mouse hindlimb muscles using
256 Fluorescence Activated Cell Sorting (FACS) as previously described[15]. Briefly, mice were
257 humanely euthanized, and their hindlimb muscles were removed and placed in a GentleMACS
258 dissociation tube (Miltenyi Biotec, #130-096-334) containing Type 1A Collagenase (628 U/mL,
259 Sigma, #C9891) in DMEM. The tissue was then physically dissociated by running the "Skeletal
260 Muscle" program in the GentleMACS Dissociator (Miltenyi Biotec, #130-093-235). Next, the tube
261 was placed on a rotating mixer at 37 °C for 1 hr. Dispase II (0.04 U/mL, Life Technologies,
262 #17105041) was then added to the tube and the muscle was further dissociated by passing through
263 a 10 mL pipette 10 times. Afterwards, the tube was returned to the rotating mixer for 1 hr. Next,
264 the digested muscle was passed through a 21 G needle 10 times, after which 10 mL of FACS buffer
265 was added to the tube. The digested muscle was passed through a 70 µm cell strainer, followed by
266 a 40 µm cell strainer. The resulting cell slurry was centrifuged at 400 g for 15 min, after which the
267 pellet was resuspended in 1 mL of FACS buffer. Red blood cells were removed by resuspending
268 the cell pellet in red blood cell lysis buffer and incubating at room temperature for 7 min. The cells
269 were then washed with FACS buffer and centrifuged at 400 g for 15 min.
270 Next, the cells were resuspended in 1 mL FACS buffer and incubated with the following
271 antibodies for 1 hr on a rotating mixer at 4 °C: CD34-eFluor 660 (1:66), α7-integrin-PE (1:500),
272 biotinylated CD31 (1:200), CD11b (1:200), Ly6A/E (1:200), and CD45 (1:500). The cells were
273 then washed with FACS buffer, centrifuged at 400 g for 15 min, and resuspended in 1 mL FACS
274 buffer. Streptavidin-PE-Cy7 (1:200) was added to the cell suspension, which was then placed on
275 a rotating mixer at 4 °C for 30 min. The cells were then washed with FACS buffer a final time,
276 centrifuged for 15 min at 400 g, and resuspended in 1 mL FACS buffer. Finally, propidium iodide

277 (1:1000) was added to the cells, and MuSCs were enriched by FACS using the following gating
278 strategy: $CD34^+/ITGA7^+/CD45^-/CD31^-/CD11b^-/Ly6A^-/PI^-$.
279 The other method to isolate murine MuSCs from the collective mouse hindlimb muscles
280 was to use Magnetic-Activated Cell Sorting (MACS) based on the vendor protocols (Miltenyi)
281 with adaptations that we found to improve MuSC enrichment. Briefly, the mouse skeletal muscle
282 tissue was processed exactly as described for FACS isolation of MuSCs up to the red blood cell
283 lysis step. After red blood cell lysis, the remaining cells were centrifuged at 400 g for 15 min. The
284 cell pellet was resuspended in 80 µL of FACS buffer and 20 µL of the Satellite Cell Isolation Kit
285 (Miltenyi Biotec, #130-104-268). The cells were incubated for 15 min at 4 °C, after which they
286 were passed through a MACS LS column (Miltenyi Biotec, #130-042-401) mounted on a
287 QuadroMACS separator (Miltenyi Biotec, #130-091-051), and the flowthrough was collected. The
288 column was washed twice with 1 mL FACS buffer, and this wash eluate was combined with the
289 flowthrough of the cells, which was then centrifuged for 5 min at 400 g. The steps of labeling,
290 magnetic depletion and collection of the flowthrough were repeated one more time with a fresh
291 MACS LS column, to maximize the removal of non-MuSC cells. The flowthrough was centrifuged
292 at 400 g for 5 min and resuspended in 80 µL of FACS buffer. 20 µL of anti-integrin α-7 microbeads
293 (Miltenyi Biotec, #130-104-261) was added to the cell suspension and then incubated at 4 °C for
294 15 min, after which the mixture was passed through a fresh MACS LS column mounted on a
295 QuadroMACS separator, to bind MuSCs to the column. The column was washed 3 times with 1
296 mL FACS buffer, and these eluates were discarded. After the washes, the LS column was removed
297 from the magnetic separator and placed on top of a 15 mL collection tube. To collect MACS
298 isolated MuSCs, 5 mL of FACS buffer was then applied to the LS column, and the magnetically
299 labeled cells (i.e., α-7 $integrin^+$) were flushed from the column into the collection tube using the
300 plunger.
301
302 **MACS- and FACS-based $Pax7^+$ cell enrichment purity assessment**
303 To compare the purity of MuSCs isolated using FACS as compared to MACS, Pax7-nGFP mice
304 were humanely euthanized, and their muscles were processed up to the point of incubation in 1
305 mL of red blood cell lysis buffer. After lysis, 10 mL of FACS buffer was added to the cell
306 suspension, which was then evenly split into two 15 mL conical tubes. The tubes were each
307 centrifuged at 400 g for 15 min. One of the tubes was processed based on the MACS isolation

308 protocol, and the other was processed based on the FACS isolation protocol. The cells prepared
309 by each method were then analyzed, using a FACS-Aria machine, with a pressure of 20Psi (low
310 pressure) and 100 μm nozzle diameter, to determine the purity of the isolated cells, which was
311 reported as the % total GFP^+ (i.e., $Pax7^+$) cells contained in each sample. Supplementary Figure
312 3 experiments that were conducted to determine the % total GFP^+ cells enriched using a variety of
313 optimisations in the MACS protocol were analyzed using the BD Accuri™ C6 Plus Flow
314 Cytometer.
315
316 **Mini-MEndR assay**
317 To conduct mini-MEndR assays, mini-myotube templates were fabricated and then cultured in
318 MEndR DM for a period of 5 days, as described above. Towards the end of differentiation day 6,
319 prospectively isolated MuSCs were resuspended in MuSC GM (Table 2) at a concentration of
320 212,500 cells/mL. Mini-myotube templates were then carefully removed from the 96-well plate
321 using a sterile tweezer and gently placed, with their inverted side up, into the cavities of a sterile
322 custom polydimethylsiloxane (PDMS) block. The PDMS block was placed within an ethanol-
323 sterilized plastic container with a moist paper towel on the bottom to create a humidified chamber.
324 4 μL of resuspended MuSC solution (i.e., 850 cells per tissue) was dispensed onto the tissue
325 surface, and evenly spread using a sterile cell spreader. The plastic container was then sealed with
326 a tight-fitting lid and the stem cell laden myotube templates (i.e., mini-MEndR tissues) were then
327 incubated for 1 hour at 37 °C, to allow the stem cells to incorporate into the mini-myotube
328 template. Following the incubation, tissues were carefully transferred back into their respective
329 96-well plate positions containing MEndR DM supplemented with 5 ng/mL rh-FGF2, and either
330 p38α/β MAPKi or DMSO carrier control (Table 4). The media, containing MEndR DM, FGF2
331 and drug treatments, was completely replaced every other day over the next 5 days. For the
332 remaining duration of the assay, tissues were cultured in MEndR DM, and half of the media was
333 replaced every other day.
334
335 **Statistical Analysis**
336 A minimum of three biological replicates (N) were conducted with multiple technical replicates
337 (n) for most experiments as detailed in Table 5. Statistical analysis was performed using GraphPad
338 Prism 8.0 software. For comparison of two variables, statistical differences were determined by

339 unpaired Student's t-test or unpaired t-test with Welch's correction. For data with more than two
340 variables compared, a one-way ANOVA followed by Tukey's multiple comparison test was
341 utilized (Table 5). All values are expressed as mean ± standard error of the mean (SEM).
342 Significance was defined as $p \leq 0.05$.
343
344 **Results**
345 **Selection of a commercially available cell source for myotube template fabrication**
346 As a first step in establishing a workflow that removed bottlenecks in manufacturing observed in
347 the original MEndR protocol[10], we set out to select a commercially available primary human
348 myoblast cell line to remove logistical challenges associated with isolating cells from fresh patient
349 tissue samples. To do this, we differentiated three commercially available primary human
350 myoblast cell lines (Table 1) in 2D culture and compared them across a battery of metrics to select
351 lines for our study that were maximized for differentiation potential and we expected would be
352 minimized for $Pax7^+$ "reserve cell"-mediated self-repair[10,16]. Specifically, we plated primary
353 myoblasts at equivalent passage number and cultured them for 1 day under growth media (GM)
354 conditions. We then transitioned the cultures to differentiation media (DM), and on the 9th day of
355 differentiation, we fixed the cultures for analysis (Figure 1A). All three cell lines formed
356 multinucleated structures that were immunoreactive for the contractile apparatus protein,
357 sarcomeric α-actinin (SAA; Figure 1B). The 18M cell line produced SAA^+ structures that covered
358 a greater proportion of the culture surface area as compared to the other two lines (Figure 1C). We
359 found that all three cell lines performed equivalently with regards to myotube nuclear accretion
360 upon evaluating the proportion of nuclei that contributed to SAA^+ structures (Figure 1D). These
361 data, coupled with visual inspection of the SAA staining (Figure 1B), in turn suggested that the
362 18M cell line likely produces myotubes of greater diameter than those produced by the other two
363 lines. Using immunocytochemistry to visualize $Pax7^+$ cells, we found that both the 18F and 19F
364 cell lines had a greater proportion of mononucleated $Pax7^+$ 'reserve cells'[16] present in myotube
365 cultures when compared to the 18M line (Figure 1E). Finally, we confirmed that the cell lines were
366 competent to produce myotubes when resuspended in a 3D fibrin-based hydrogel and cultured in
367 a cellulose scaffold using the original myotube template manufacturing protocol (Figure 1F-H). In
368 all cases, we observed the formation of myotubes structures and similar levels of SAA-coverage
369 within the scaffold (Figure 1G-H). Since our prior studies suggested that high reserve cell content

370 can mask the regenerative influence of muscle stem cells added to the assay[10], we elected to move
371 forward with the 18M and 19F lines and abandon the 18F line for this study.
372
373 **Cellulose scaffolds pre-adsorbed with thrombin to allow scalable manufacturing**
374 Having selected commercial cell lines, we set out to establish a workflow for production of
375 myotube templates in a manner that mitigated time-sensitive steps in the original fabrication
376 protocol that we have observed prove challenging for new users that want to adopt the MEndR
377 platform. In the original protocol, myogenic progenitors were resuspended within a fibrinogen /
378 thrombin / Geltrex™ based hydrogel precursor solution, which was subsequently manually
379 distributed over the cellulose scaffold to evenly spread the hydrogel suspensions and encourage
380 infiltration into the scaffold pores prior to hydrogel gelation[10]. A fibrin clot (i.e., hydrogel) forms
381 rapidly upon combining the fibrinogen with thrombin, allowing only a short window of time to
382 resuspend the myogenic progenitors within the solution, dispense the gel-cell solution onto the
383 scaffold, and infiltrate into the cellulose pores. When fabricating only a small (<24) number of
384 scaffolds, this time window is a minimal problem. However, we were concerned that when
385 fabricating 96-scaffolds, this short time window would present a significant challenge. To
386 decouple the hydrogel mixing and gelation steps, we assessed if we could adsorb thrombin (which
387 initiates fibrin gelation), to the cellulose scaffold (Figure 2A). We reasoned that using this
388 approach the myogenic progenitor / fibrinogen / Geltrex™ solution would polymerize in situ only
389 upon making contact with the thrombin-adsorbed cellulose scaffold. We first wanted to confirm
390 that pre-adsorbing fibrin on the scaffold resulted in hydrogel gelation upon infiltration into the
391 scaffold. To this end, we mixed fluorescent beads into the fibrinogen / thrombin / Geltrex™
392 hydrogel precursor solution, infiltrated the solution into the pre-adsorbed scaffold and allowed
393 gelation, imaged the beads, washed vigorously to rinse out any unpolymerized hydrogel (and
394 beads), and then re-imaged the remaining beads to allow us to quantify bead loss due to the
395 washing step (Figure 2A-C). As expected, when no thrombin was present, bead loss occurred upon
396 washing the scaffolds. In conditions where thrombin was directly mixed into the pre-cursor
397 solution, or pre-adsorbed onto the cellulose scaffold, minimal bead loss was observed (Figure 2B-
398 C).
399 When we used this pre-adsorption protocol with myoblasts rather than beads, within one
400 week of culture, we observed thin sheets of multinucleated myotubes form across the two cell lines

401 tested (Figure 2D-E). Further, the proportion of 3D tissues covered by SAA^+ myotubes in myotube
402 templates formed using pre-adsorption of thrombin to the scaffold was similar to those formed
403 when thrombin was directly mixed in (Figure 2E-F). We therefore conclude that the pre-adsorption
404 of the thrombin in the cellulose scaffold enabled robust manufacturing of muscle templates that
405 differentiated as expected.
406
407 **Fabrication of myotube templates within a 96-well footprint**
408 We next set out to manufacture MEndR tissues compatible with a 96-well plate footprint. To
409 miniaturize myotube templates from the original 24-well rectangular format[10], we cut sheets of
410 cellulose teabag paper into circular discs using a 5 mm circular biopsy punch (Figure 3A). The
411 circular cellulose scaffolds were autoclaved and then placed into pluronic acid treated wells of a
412 96-well plate using anti-static tweezers. The pluronic acid treatment discouraged myoblast
413 migration or attachment beyond the boundary of the scaffold (Supplementary Figure 1). For both
414 of the myoblast cell lines, we observed formation of multinucleated myotubes by day 7 of
415 differentiation and similar levels of SAA tissue coverage at days 10 and 14 of culture, at which
416 point, we concluded the experiment (Figure 3B-D). SAA tissue coverage at day 7 in the
417 miniaturized format (Figure 3C-D) was similar to that observed in the large format at day 8 for
418 both cell lines (Figure 1H versus Figures 3C and D). Importantly, we found that, in general, three
419 rounds of practice seeding the 96-well format myotube templates using the optimized protocol was
420 sufficient for new users to master the method (Supplementary Figure 2). We therefore concluded
421 that myotube templates could be generated in this smaller dimension format and that new users
422 with myoblast cell culture experience can quickly become proficient with the method.
423
424 **Miniaturized myotube templates possess limited self-repair capacity**
425 Having miniaturized our myotube template platform into a 96-well format, we next set out to
426 demonstrate that our miniaturized platform supported the stem cell mediated repair workflow.
427 Specifically, we wanted to confirm that the miniaturized myotube templates were susceptible to
428 damage induced by cardiotoxin, a snake venom toxin commonly used to induce muscle damage in
429 mouse studies[17]. To do this, on day 7 of mini-myotube template culture, we introduced cardiotoxin
430 to the culture media (Figure 4A). Mini-myotube templates were fixed 24 hrs after the initial
431 cardiotoxin exposure and immunostained to visualize and quantify the resulting SAA^+ myotube

432 structures (Figure 4A-D). We observed a 21.31% +/- 4.37% and 24.12% +/- 5.24% decrease in
433 SAA immunoreactivity one day after cardiotoxin treatment in myotube templates generated from
434 the 18M and 19F myoblast lines, respectively (Figure 4C-D), consistent with prior results obtained
435 using the larger myotube template format[10].
436 We next analyzed the mini-myotube templates 10 days after cardiotoxin exposure, to
437 determine whether Pax7^{+} reserve cell activity alone regenerated the injured myotube templates
438 (Figure 5A). Similar to the larger myotube template format[10], we found that the SAA content failed
439 to return to levels observed in the uninjured control (Figures 5B-D, DMSO CTX(-) vs CTX (+)).
440 As expected, when templates were treated with an inhibitor of p38 α/β MAP kinase (p38i), a
441 treatment known to expand both muscle stem and progenitor cells[8], we observed that SAA content
442 was able to return to levels matching the uninjured control (Figure 5B-D). By contrast, treatment
443 with an epidermal growth factor receptor inhibitor (EGFRi) failed to stimulate reserve cell-
444 mediated myotube template repair, as measured by SAA coverage (Figure 5B-D). Together, these
445 results confirmed that the mini-myotube templates were receptive to injury, and had limited self-
446 repair capacity, allowing for enhancement by engrafting freshly isolated MuSCs.
447
448 **A MACS-based MuSC enrichment strategy supports MEndR assay scale-up**
449 We next set out to demonstrate that muscle stem cell mediated skeletal muscle tissue repair occurs
450 in the miniaturized myotube template format. We previously showed that freshly FACS-sorted
451 MuSCs introduced to injured myotube templates contribute to the process of tissue repair by
452 producing new myotubes[10]. For these studies, we prospectively isolated MuSCs from
453 enzymatically digested murine skeletal muscle tissue using a magnetic-activated cell sorting
454 (MACS) strategy (Supplementary Figure 3), which we first confirmed to produce similar results
455 as compared to MuSCs isolated using a traditional fluorescence activated cell sorting (FACS)
456 protocol (Supplementary Figure 4). For this comparison, we harvested hindlimb skeletal muscle
457 tissue from humanely euthanized Pax7-nGFP transgenic reporter mice (Supplementary Figure 3)
458 or those ubiquitously expressing yellow fluorescent protein (YFP; Supplementary Figure 4) and
459 subjected it to standard mechanical dissociation and enzymatic digestion protocols to produce a
460 single cell suspension. The cell suspension was split equally, processed, and sorted
461 (Supplementary Figure 3A) using either a FACS (Supplementary Figure 3B-C) or MACS-based
462 protocol (Supplementary Figure 3C-D). The cell populations harvested from Pax7-nGFP animals

463 were characterized immediately after enrichment using flow cytometry (Supplementary Figure
464 3C). We found that 97.87% +/- 2.24% of events from FACS-enriched events were GFP^+, whereas
465 91.70% +/- 0.97% of events were GFP^+ following a modified MACS enrichment strategy that
466 employed two-rounds of lineage depletion (Supplementary Figure 3C-D). We speculated that the
467 greater proportion of GFP-negative cells within the MACS-enriched cell population could be owed
468 to integrin α-7^+ contaminating cell types[18], or that it may be an artifact of magnetic-enrichment
469 protocols which are less effective than FACS at removing cellular debris. In prior studies, we
470 plated the FACS and MACS-enriched cell populations in culture and then 12 hrs later, enumerated
471 the viable GFP positive and negative cells in each well[19]. This uncovered a dramatic loss of the
472 GFP-negative population from the MACS-enriched cell population, resulting in an enrichment for
473 GFP-positive cells that matched values obtained using FACS-enrichment. As expected, increased
474 experience using the MACS method correlates with a consistently higher proportion of GFP^+ cells
475 in the populations enriched from Pax7-nGFP transgenic animals (data not shown). It is also worth
476 noting that in our experience MACS-based enrichment consistently offered higher cell yields when
477 compared to the FACS-based strategy (data not shown). Together this data suggested that MACS
478 was a feasible and convenient method for sorting MuSCs from mouse hindlimb skeletal muscle
479 tissue for our scaled MEndR assay.
480
481 **Miniaturized format supports muscle endogenous repair (mini-MEndR) assays**
482 We next wanted to confirm that our miniaturized myotube template system, seeded with MuSCs,
483 could replicate key results observed using the original MEndR assay which successfully identified
484 and recapitulated outcomes of known stimulators of murine muscle stem cell mediated muscle
485 tissue repair[10]. We generated myotube templates, and then on day 6 of differentiation we
486 introduced MACS enriched MuSCs from YFP-transgenic animals. 12 hr after MuSC engraftment,
487 co-cultures were then exposed to cardiotoxin to injure the myotube templates, after which we
488 introduced to the culture media a p38 α/β MAPK inhibitor (p38i), a known modulator of stem cell
489 skeletal mediated repair, or DMSO carrier control. At 7 or 10 days post-injury (DPI), the tissues
490 were fixed and immunostained to evaluate the donor-derived contributions to muscle tissue repair
491 (Figure 6A-B). Consistent with our results in the large MEndR format, we observed increased
492 donor derived myotube formation in tissues treated with p38i, suggesting enhanced stem cell
493 mediated repair that was apparent at 10 DPI (Figure 6C-D). This effect was observed when MuSCs

494 were introduced to myotube templates generated from both the 18M and 19F primary myoblasts
495 (Figure 6C-D). Further, MuSCs prospectively isolated using the MACS-enrichment method
496 performed in a functionally equivalent manner by this metric when compared against those sorted
497 using a classic FACS-based method (Supplementary Figure 4). The effect of p38i on donor
498 myotube production was statistically detectable by 7 DPI, and was not significantly different from
499 the results obtained at 10 DPI. This observation suggests that a shortened timeline to assess stem
500 cell-mediated muscle production using the mini-MEndR assay is feasible, benefiting future
501 screening applications.

502 We next assessed another key read-out of stem cell mediated skeletal muscle repair, niche
503 repopulation, which we have shown is captured in the original MEndR format[10]. For these studies,
504 we repeated the protocol described above, using instead MuSCs isolated from Pax7-nGFP
505 transgenic reporter animals (Figure 7A). On day 7 post-injury, when tissue repair was complete,
506 we observed a population of mononucleated Pax7$^+$ donor-derived (GFP; Figure 7B), which we
507 previously showed had reversibly exited cell cycle[10]. Further, and in line with results obtained in
508 the original MEndR platform, we observed a ~3-fold increase in these donor-derived Pax7$^+$ cells
509 in response to p38i treatment (Figure7C-D). The MEndR and mini-MEndR assays were designed
510 as a mixed species cell 'competition' assay in part to enable multiplexed analyses of human and
511 mouse Pax7$^+$ populations within the same assay. The mouse Pax7$^+$ cell population is isolated from
512 a transgenic animal and therefore easily distinguished from the unlabeled Pax7$^+$ 'reserve cells' that
513 exist within the primary human myoblast population, which is used to fabricate the myotube
514 template. Thus, enumerating the mononucleated Pax7 immunoreactive cells present in the
515 myotube template at the end-point of a mini-MEndR assay, while tracking whether they are GFP
516 labeled (mouse) or unlabeled (human) enables a cursory assessment of species specific Pax7$^+$ cell
517 responses. Consistently, when we enumerated the Pax7$^+$ reserve cell abundance at the assay end-
518 point, treatment with the p38i produced an increase in the incidence of mononucleated Pax7$^+$
519 reserve cells (Figure 7E-F).

520 Together this data suggested that the miniaturized muscle endogenous repair assay (mini-
521 MEndR) replicates all of the stem cell functional metrics previously reported in the original large
522 format MEndR assay.

523

524 **Discussion**

525 In this paper we set out to miniaturize and improve the manufacturing workflow of our
526 previously reported skeletal muscle stem cell mediated repair assay, known as MEndR[10], to
527 enable wider adoption of this powerful assay to identify novel molecular targets that promote
528 muscle regeneration. We addressed three critical bottlenecks in the workflow of the original
529 MEndR assay, that have up until now limited its capacity to assess molecular targets at a
530 practically useful scale. Firstly, we demonstrate use of primary human myoblasts from a
531 commercial source to generate the myotube template to reduce myotube template variation
532 associated with the use of different muscle biopsy donors. Second, we developed a method to
533 integrate the hydrogel crosslinker into the scaffold to trigger in situ gelation to counter the rapid
534 gelation properties of the fibrin hydrogel used to manufacture the myotube template, which had
535 limited the number of myotube templates that can be robustly manufactured using one batch of
536 myoblast-hydrogel suspension. Third, we validate the use of an alternative to FACS for sorting
537 skeletal muscle stem cells from digested skeletal muscle which overcomes limits on the number
538 of wells that can be assessed in parallel using freshly isolated adult stem cells. Further, we
539 miniatured the format of the assay ~6-fold to reduce both the number of template cells and added
540 stem cells required per well to perform the assay, and demonstrated the possibility of a shorter
541 assay endpoint.
542 The use of cross-linker adsorption to the paper scaffold to enable in situ hydrogel gelation
543 during tissue manufacturing was particularly critical to able scalable manufacturing of the
544 myotube template due to the rapid gelation of fibrin upon addition of the thrombin crosslinker to
545 the bulk hydrogel solution containing the myoblasts. We anticipate this innovation could enable
546 the manufacturing of myotube templates using robotic liquid handling in the future to support
547 tissue manufacturing for large scale screening efforts. Indeed this strategy could potentially be
548 utilized to generate tissues for other applications that use two component hydrogels in which gel
549 crosslinking is initiated by the addition of an external crosslinking component as opposed to
550 simply a temperature change alone. Interestingly, we observed that the use of thrombin pre-
551 adsorption dramatically reduced the number of attempts required to master the mini-MEndR
552 seeding protocol, which suggests that pre-mature hydrogel gelation could be a key source of
553 inter-well variation in other paper-based systems[13,20].
554 While this work successfully increased the throughput capacity of our MEndR assay to
555 enable potential screening of drug candidates at a 96-well plate scale, it is important to note some

556 remaining limitations of the mini-MEndR assay. We note that removal of the myotube template
557 from each well to integrate the muscle stem cells remains a rate limiting step in our work flow.
558 However, this step does not significantly impact usability at a 96-well plate throughput. A 96-
559 well throughput is appropriate for assessing 10s to 100s of targets. This manual removal step,
560 however would limit use of robots in fully automating our assay. If a larger scale screening
561 capacity is desirable in the future, the MEndR assay could be further integrated with the SPOT
562 platform[20], reported by our group, which we recently demonstrated is compatible with robotic
563 liquid handler to enable massive increases in scale[21].
564 Given that the myotube template contains a population of Pax7$^+$ reserve cells that have
565 the potential to contribute to myotube template repair, even in the absence of adding a MuSC
566 population, means that readouts of mini-MEndR SAA-coverage alone are not able to distinguish
567 between drugs that target this reserve cell population versus those that target the MuSC
568 population specifically. Thus, it is important for MuSCs that are added to mini-MEndR
569 experiments to be fluorescently labeled to disentangle MuSC and template reserve cell
570 regenerative activities. An advantage of conducting mixed species mini-MEndR experiments is
571 the ability to track the influence of treatments on both human Pax7$^+$ reserve cell and mouse
572 MuSC self-renewal and differentiation within the same experiment. The user has complete
573 control over MuSC content in each experiment, but limited control over the drift in Pax7$^+$ reserve
574 cell content. Further, there is ongoing debate with regards to drawing conclusions about human
575 MuSC biology based solely on human Pax7$^+$ reserve cell studies. For example, the EGFRi
576 treatment induced different effects on mouse MuSCs as compared to human Pax7$^+$ reserve cells
577 based upon our experiments, and whether this reflects an influence of species or is a MuSC vs
578 reserve cell difference has yet to be determined. Thus, downstream studies to evaluate the effects
579 of 'hits' on bonefide human MuSCs are to be expected, and adaptions of the assay to integrate
580 MuSC freshly enriched from human muscle biopsies are underway. The capacity to conduct
581 follow up experiments at a higher scale in combination with the compatibility of mini-MEndR
582 tissues to be imaged semi-automatically with high-content imaging systems will serve to
583 facilitate follow up dose response and mechanistic studies of molecular targets identified in the
584 initial screen.
585
586 **Conclusions**

587 Identification of drugs to boost the capacity of MuSCs to drive skeletal muscle endogenous repair
588 is an exciting approach to address various conditions that lead to impaired skeletal muscle
589 regeneration, such as aging or DMD. The MEndR assay provides a powerful functional assay "in
590 a dish" with the potential to shortlist molecular targets that enhance human skeletal muscle
591 endogenous repair. Here we adapted the original MEndR manufacturing workflow to enable the
592 robust manufacturing of a 96-well plate "mini-MEndR" platform. Further we validated that this
593 miniaturized platform recapitulates the known endogenous repair readouts captured in the original
594 larger MEndR format. The mini-MEndR platform has the potential to enable the identification of
595 novel molecular targets to modulate stem-cell mediated skeletal muscle repair and to facilitate an
596 exploration of their cellular and molecular mechanism(s) of action.
597

598 **Acknowledgements**

599 N.G., S.D., and B.X. contributed equally to this work. S.R., and E.J. contributed equally to this
600 work. BioRender was utilized to produce schemata elements. This project was funded by a Canada
601 First Research Excellence Fund "Medicine by Design (MbD)" grant to P.M.G. and A.P.M.
602 (MbDC2-2019-02), a Natural Sciences and Engineering Research Council of Canada (NSERC)
603 Idea to Innovation grant awarded to A.P.M. and P.M.G. (I2IPJ 549768-20), a University of
604 Toronto Connaught Fund awarded to A.P.M. and P.M.G., a Canada Research Chair in Endogenous
605 Repair award to P.M.G. (#950-231201), Stem Cell Network grant to P.M.G. (#FY20/DRP-1),
606 Ontario Institute for Regenerative Medicine grant to P.M.G. (#2018-0510), CGS-D Awards to B.X.
607 and E.J., a CGS-M Award to S.R., an NSERC CREATE TOeP scholarship to S.D., Ontario
608 Graduate Scholarships to B.X., S.R., and E.J. and a Norman F. Moody Award to B.X.
609

610 **Author contributions**

611 N.G., S.D., B.X., S.R., E.J., J.P., and A.F. designed and performed research, analyzed data, and
612 prepared figures. A.P.M., P.M.G., and S.D. conceived of the project and supervised the research.
613 All authors contributed to data interpretation. A.P.M., P.M.G., N.G., B.X., and S.R. wrote the
614 manuscript. All authors reviewed and approved the manuscript.
615

616 **Conflict of Interest**

The authors have no competing interests, or other interests that might be perceived to influence the results and/or discussion reported in this paper.

Data and Materials Availability Statement

The datasets generated during and analyzed in this study are available from the corresponding author on reasonable request.

References

(1) Brunet, A.; Goodell, M. A.; Rando, T. A. Ageing and Rejuvenation of Tissue Stem Cells and Their Niches. *Nat. Rev. Mol. Cell Biol.* **2023**, *24* (1), 45–62. https://doi.org/10.1038/s41580-022-00510-w.

(2) Dumont, N. A.; Wang, Y. X.; Von Maltzahn, J.; Pasut, A.; Bentzinger, C. F.; Brun, C. E.; Rudnicki, M. A. Dystrophin Expression in Muscle Stem Cells Regulates Their Polarity and Asymmetric Division. *Nat. Med.* **2015**, *21* (12), 1455–1463. https://doi.org/10.1038/nm.3990.

(3) Wang, Y. X.; Feige, P.; Brun, C. E.; Hekmatnejad, B.; Dumont, N. A.; Renaud, J. M.; Faulkes, S.; Guindon, D. E.; Rudnicki, M. A. EGFR-Aurka Signaling Rescues Polarity and Regeneration Defects in Dystrophin-Deficient Muscle Stem Cells by Increasing Asymmetric Divisions. *Cell Stem Cell* **2019**, *24* (3), 419—-432.e6. https://doi.org/10.1016/j.stem.2019.01.002.

(4) Rozo, M.; Li, L.; Fan, C. M. Targeting B1-Integrin Signaling Enhances Regeneration in Aged and Dystrophic Muscle in Mice. *Nat. Med.* **2016**, *22* (8), 889–896. https://doi.org/10.1038/nm.4116.

(5) Porpiglia, E.; Mai, T.; Kraft, P.; Holbrook, C. A.; de Morree, A.; Gonzalez, V. D.; Hilgendorf, K. I.; Frésard, L.; Trejo, A.; Bhimaraju, S.; Jackson, P. K.; Fantl, W. J.; Blau, H. M. Elevated CD47 Is a Hallmark of Dysfunctional Aged Muscle Stem Cells That Can Be Targeted to Augment Regeneration. *Cell Stem Cell* **2022**, *29* (12), 1653-1668.e8. https://doi.org/10.1016/j.stem.2022.10.009.

(6) Benjamin, D. I.; Both, P.; Benjamin, J. S.; Nutter, C. W.; Tan, J. H.; Kang, J.; Machado, L. A.; Klein, J. D. D.; de Morree, A.; Kim, S.; Liu, L.; Dulay, H.; Feraboli, L.; Louie, S. M.; Nomura, D. K.; Rando, T. A. Fasting Induces a Highly Resilient Deep Quiescent State in Muscle Stem Cells via Ketone Body Signaling. *Cell Metab.* **2022**, *34* (6), 902-918.e6. https://doi.org/10.1016/j.cmet.2022.04.012.

(7) Gilbert, P. M.; Havenstrite, K. L.; Magnusson, K. E. G.; Sacco, A.; Leonardi, N. A.; Kraft, P.; Nguyen, N. K.; Thrun, S.; Lutolf, M. P.; Blau, H. M. Substrate Elasticity Regulates Skeletal Muscle Stem Cell Self-Renewal in Culture. *Science* **2010**, *329* (5995), 1078–1081. https://doi.org/10.1126/science.1191035.

(8) Cosgrove, B. D.; Gilbert, P. M.; Porpiglia, E.; Mourkioti, F.; Lee, S. P.; Corbel, S. Y.; Llewellyn, M. E.; Delp, S. L.; Blau, H. M. Rejuvenation of the Muscle Stem Cell Population Restores Strength to Injured Aged Muscles. *Nat. Med.* **2014**, *20* (3), 255–264. https://doi.org/10.1038/nm.3464.

(9) Sacco, A.; Doyonnas, R.; Kraft, P.; Vitorovic, S.; Blau, H. M. Self-Renewal and Expansion of Single Transplanted Muscle Stem Cells. *Nature* **2008**, *456* (7221), 502–506. https://doi.org/10.1038/nature07384.

(10) Davoudi, S.; Xu, B.; Jacques, E.; Cadavid, J. L.; McFee, M.; Chin, C.-Y.; Meysami, A.; Ebrahimi, M.; Bakooshli, M. A.; Tung, K.; Ahn, H.; Ginsberg, H. J.; McGuigan, A. P.; Gilbert, P. M. MEndR: An in Vitro Functional Assay to Predict in Vivo Muscle Stem Cell-Mediated Repair. *Adv. Funct. Mater.* **2021**.

(11) Fleming, J. W.; Capel, A. J.; Rimington, R. P.; Wheeler, P.; Leonard, A. N.; Bishop, N. C.; Davies, O. G.; Lewis, M. P. Bioengineered Human Skeletal Muscle Capable of Functional Regeneration. *BMC Biol.* **2020**, *18* (1), 145. https://doi.org/10.1186/s12915-020-00884-3.

(12) Wang, J.; Broer, T.; Chavez, T.; Zhou, C. J.; Tran, S.; Xiang, Y.; Khodabukus, A.; Diao, Y.; Bursac, N. Myoblast Deactivation within Engineered Human Skeletal Muscle Creates a Transcriptionally Heterogeneous Population of Quiescent Satellite-like Cells. *Biomaterials* **2022**, *284*, 121508. https://doi.org/10.1016/j.biomaterials.2022.121508.

(13) Rodenhizer, D.; Dean, T.; Xu, B.; Cojocari, D.; McGuigan, A. P. A Three-Dimensional Engineered Heterogeneous Tumor Model for Assessing Cellular Environment and Response. *Nat. Protoc.* **2018**, *13* (9), 1917–1957. https://doi.org/10.1038/s41596-018-0022-9.

(14) Sambasivan, R.; Gayraud-Morel, B.; Dumas, G.; Cimper, C.; Paisant, S.; Kelly, R. G.; Tajbakhsh, S. Distinct Regulatory Cascades Govern Extraocular and Pharyngeal Arch Muscle Progenitor Cell Fates. *Dev Cell* **2009**, *16* (6), 810–821. https://doi.org/10.1016/j.devcel.2009.05.008 S1534-5807(09)00210-X [pii].

(15) Davoudi, S.; Chin, C.-Y.; Cooke, M. J.; Tam, R. Y.; Shoichet, M. S.; Gilbert, P. M. Muscle Stem Cell Intramuscular Delivery within Hyaluronan Methylcellulose Improves Engraftment Efficiency and Dispersion. *Biomaterials* **2018**, *173*, 34–46. https://doi.org/10.1016/j.biomaterials.2018.04.048.

(16) Laumonier, T.; Bermont, F.; Hoffmeyer, P.; Kindler, V.; Menetrey, J. Human Myogenic Reserve Cells Are Quiescent Stem Cells That Contribute to Muscle Regeneration after Intramuscular Transplantation in Immunodeficient Mice. *Sci. Rep.* **2017**, *7* (1), 3462. https://doi.org/10.1038/s41598-017-03703-y.

(17) Hardy, D.; Besnard, A.; Latil, M.; Jouvion, G.; Briand, D.; Thépenier, C.; Pascal, Q.; Guguin, A.; Gayraud-Morel, B.; Cavaillon, J. M.; Tajbakhsh, S.; Rocheteau, P.; Chrétien, F. Comparative Study of Injury Models for Studying Muscle Regeneration in Mice. *PloS One* **2016**, *11* (1), e0147198. https://doi.org/10.1371/journal.pone.0147198.

(18) Giordani, L.; He, G. J.; Negroni, E.; Sakai, H.; Law, J. Y. C.; Siu, M. M.; Wan, R.; Corneau, A.; Tajbakhsh, S.; Cheung, T. H.; Le Grand, F. High-Dimensional Single-Cell Cartography Reveals Novel Skeletal Muscle-Resident Cell Populations. *Mol. Cell* **2019**, *74* (3), 609-621.e6. https://doi.org/10.1016/J.MOLCEL.2019.02.026.

(19) Jacques, E.; Kuang, Y.; Kann, A. P.; Le Grand, F.; Krauss, R. S.; Gilbert, P. M. The Mini-IDLE 3D Biomimetic Culture Assay Enables Interrogation of Mechanisms Governing Muscle Stem Cell Quiescence and Niche Repopulation. *eLife* **2022**, *11*, e81738. https://doi.org/10.7554/eLife.81738.

(20) Li, N. T.; Wu, N. C.; Cao, R.; Cadavid, J. L.; Latour, S.; Lu, X.; Zhu, Y.; Mijalkovic, M.; Roozitalab, R.; Landon-Brace, N.; Notta, F.; McGuigan, A. P. An Off-the-Shelf Multi-Well Scaffold-Supported Platform for Tumour Organoid-Based Tissues. *Biomaterials* **2022**, *291*, 121883. https://doi.org/10.1016/j.biomaterials.2022.121883.

704 (21) Cao, R.; Li, N. T.; Cadavid, J. L.; Latour, S.; Tan, C. M.; McGuigan, A. P. *An Automation*
705 *Workflow for High-Throughput Manufacturing and Analysis of Scaffold-Supported 3D*
706 *Tissue Arrays*; preprint; Bioengineering, 2022. https://doi.org/10.1101/2022.08.20.504600.
707

708 **Figure Legends**

709 **Figure 1. Characterization of commercially available human pMB lines. (A)** Experimental
710 timeline for the 2D differentiation of the human primary myoblasts. **(B)** Representative 10X
711 confocal images of the three commercially available human myoblasts immunostained for
712 sarcomeric α-actinin (SAA; magenta) and counterstained for DRAQ5 (grey) on day 9 of
713 differentiation in 2D culture. Scale bar, 500 µm. **(C-E)** Bar graphs quantifying SAA coverage **(C)**,
714 average nuclear fusion index **(D)**, and ratio of $Pax7^+$ reserve cells amongst the mononuclear cells
715 **(E)** in 2D culture on day 9 differentiation comparing the three cell lines. Graphs display mean ±
716 s.e.m., one-way ANOVA with Tukey post-test. ** $p < 0.01$, *** $p < 0.001$, **** $p < 0.0001$, ns. -
717 no significance. n=3 wells from N=1 experiment per cell line. **(F)** Schematic of the 24-well
718 myotube template derivation workflow. **(G)** Representative confocal images of SAA (magenta)
719 immunostaining in myotube templates at day 8 of differentiation that were generated using the
720 18M, 18F and 19F cell lines. Scale bar, 500 µm. **(H)** Bar graph quantification of myotube template
721 SAA coverage at day 8 of differentiation. Graphs display mean ± s.e.m., one-way ANOVA with
722 Tukey post-test, ns. – no significance. n=2 tissues from N =1 experiment per cell line.
723

724 **Figure 2. Preabsorbing thrombin in paper scaffolds to facilitate myotube template seeding.**
725 **(A)** Schematic of the bead assay workflow. Cellulose scaffolds were pre-adsorbed with thrombin
726 and seeded with fluorescent beads diluted 10 times in ECM master mix. The beads were imaged
727 before and after washing to quantify bead retention. **(B)** Representative confocal images of bead
728 assay paper scaffolds before and after washing. Scale bar, 500 µm. **(C)** Quantification of the
729 number of beads before washing (black) and after washing (grey) for fluorescent beads seeded on
730 paper scaffolds without thrombin, with 0.8 U/ml thrombin mixed-in, or with 0.8 U/ml thrombin
731 pre-adsorption. Graphs display mean ± s.e.m., two-way ANOVA followed by Sidak's multiple
732 comparisons test *** $p < 0.001$, N=2, n=8. **(D)** Experimental workflow for comparing thrombin
733 mixed-in (left) to pre-adsorption (right) methods on myotube template formation. **(E)**
734 Representative confocal images of myotube template stained for phalloidin (magenta) after 7 days
735 of differentiation. Scale bar, 500 µm. **(F)** Quantification of phalloidin coverage for thrombin

736 mixed-in vs pre-adsorption methods. ns. = no significance. n=11-24 tissues from N=3-4
737 independent experiments.
738
739 **Figure 3**. **Mini-myotube template derivation. (A)** Schematic of the mini-myotube template
740 derivation workflow. Cellulose scaffolds were pre-adsorbed with thrombin and seeded with human
741 pMBs mixed in an ECM mixture containing DMEM, fibrinogen and Geltrex^{TM}. **(B)** Representative
742 confocal images of SAA (magenta) immunostaining for mini-myotube templates generated with
743 the 18M and 19F cell lines and analyzed on days 7, 10, and 14 of differentiation. Scale bar, 500
744 µm. **(C, D)** Quantification of SAA coverage in mini-myotube templates generated with the 18M
745 **(C)** and 19F **(D)** cell lines on days 7, 10, and 14 of differentiation. Graphs display mean ± s.e.m.
746 one-way ANOVA with Tukey post-test. * $p < 0.05$, ** $p < 0.01$ ns. = no significance. n = 6-10
747 tissues from N = 3-4 independent experiments per cell line.
748
749 **Figure 4. Myotoxin-induced mini-myotube templates injury. (A)** Schematic of the template
750 injury workflow. Mini-myotube templates are incubated in MEndR differentiation media
751 containing 0.5 µm cardiotoxin (CTX) for 4 hr at 37 °C on an orbital shaker. **(B)** Representative
752 confocal images of uninjured (left; (-)) and injured (right; (+)) mini-myotube templates generated
753 with the 18M (top) or 19F (bottom) cell lines (SAA; magenta) at 1 DPI. Scale bar, 500 µm. **(C,**
754 **D)** Quantification of SAA tissue coverage in uninjured and injured mini-myotube templates
755 generated with 18M **(B)** or 19F **(C)** cell lines at 1 DPI. Graphs display mean ± s.e.m. Unpaired
756 student's t-test, **** $p < 0.0001$. n =11-20 tissues from N=5-6 independent experiments per cell
757 line.
758
759 **Figure 5. p38α/β MAPKi, but not EGFRi, induces mini-myotube template self-repair. (A)**
760 Experimental timeline to study mini-myotube template self-repair capacity. **(B)** Representative
761 confocal images of uninjured (CTX(-)) and injured (CTX(+)) myotube templates generated with
762 18M (top) or 19F (bottom) cell lines in response to treatment with p38α/β MAPK inhibitor (p38i),
763 epidermal growth factor inhibitor (EGFRi) or DMSO carrier control at 10 DPI. Scale bar, 500 µm.
764 **(C, D)** Quantification of SAA coverage in uninjured and injured myotube templates generated with
765 18M **(C)** or 19F **(D)**. Graphs display mean ± s.e.m. one-way ANOVA with Tukey post-test, *

766 p<0.05, ** p < 0.01, *** p < 0.001, **** p < 0.0001. n =10-15 tissues from N=4-5 independent
767 experiments per cell line.
768
769 **Figure 6. p38α/β MAPKi treatment augments MuSC-mediated muscle production in mini-**
770 **MEndR assay. (A)** Schematic of the mini-MEndR assay workflow. MuSCs from YFP transgenic
771 mice are isolated using the adapted magnetic assisted cell sorting (MACS) protocol and then
772 engrafted onto the mini-myotube templates on day 6 of differentiation, followed by drug
773 treatments and cardiotoxin-induced tissue injury. **(B)** Detailed experimental timeline for the mini-
774 MEndR assay workflow. **(C)** Representative confocal images of MuSC-mediated (YFP^+) myotube
775 production in the injured mini-myotube templates produced with 18M (top panel) 19F (bottom
776 panel) in response to treatment with DMSO or p38α/β MAPKi harvested at 7 DPI. Scale bar, 500
777 µm. (**D-E)** Quantification of the MuSC-mediated regeneration (%YFP coverage) in the injured
778 mini-myotube templates generated with 18M **(D)** or 19F **(E)** cell line harvested at 7 DPI or 10 DPI.
779 Graphs display mean± s.e.m; Unpaired two-tailed T-test with Welch's correction was conducted
780 for each condition. * p<0.05, ** p < 0.001, **** p, n=9-12 tissues from N=3-4 independent
781 experiments per cell line.
782
783 **Figure 7. mini-MEndR assay captures response of treatment known to stimulate MuSC self-**
784 **renewal. (A)** Detailed experimental timeline of donor-derived MuSC niche repopulation. **(B)**
785 Representative confocal images of $Pax7^+GFP^+$ donor derived MuSCs in mini-MEndR tissues
786 treated with p38α/β MAPKi at 7 DPI. Tissues are immunostained for Pax7 (grey), GFP (green),
787 and DAPI (cyan). Magenta arrowheads point to the $Pax7^+$ GFP^+ donor MuSCs and yellow
788 arrowheads point to the $Pax7^+$ GFP^- reserve cells derived from the myotube template. Scale bar,
789 50 µm. **(C-F)** Quantification of $Pax7^+$ GFP^+ cells derived from donor MuSCs (**C-D**) or $Pax7^+$ GFP^-
790 reserve cells derived from the myotube template (**E-F**) in mini-MEndR tissues generated with 18M
791 **(C, E)** and 19F **(D, F)** cell lines, following treatment with DMSO or p38α/β MAPKi in the context
792 of injury and analyzed at 7 DPI. Graphs display mean ± s.e.m.; Unpaired two-tailed T-test with
793 Welch's correction. * p < 0.5, *** p < 0.001, **** p < 0.0001. n=6-9 tissues from N=3 independent
794 experiments per cell line.
795
796 **Supplementary Figure Legends**

797 **Supplementary Figure 1. Pluronic acid coating allows for the generation of smooth mini-**
798 **myotube template edges.** Representative confocal images of mini-myotubes generated with (+)
799 and without (-) pluronic acid coating. Tissues are immunostained for sacromeric α-actinin (SAA;
800 magenta). Scale bar, 1 mm.
801
802 **Supplementary Figure 2. Mini-MEndR platform manufacture can be quickly mastered by**
803 **new users. (A)** Representative confocal images of myotube templates generated by the same user
804 at different levels of experience. Tissues were fixed after 7 days of differentiation and stained with
805 phalloidin (magenta). Scale bar, 500 µm. **(B)** Quantification of Phalloidin (User 1) or SAA (User
806 2, 3) tissue coverage attained by three different users who trained from first-time user to expert
807 level as indicated by plateauing coverage and homogeneous mini-myotube templates. Coverage
808 was normalized to the average of each user's three most recent seeding attempts at expert level to
809 account for cell line-to-cell line differences in absolute fiber coverage.
810
811 **Supplementary Figure 3. Gating strategy used for MACS or FACS based MuSCs isolation.**
812 **(A)** Schematic showcasing the workflow of MACS vs FACS MuSC isolation protocols. **(B)** Flow
813 cytometry plots demonstrating gating strategy to enrich MuSCs from Pax7-nGFP transgenic mice
814 using FACS. **(C)** Representative plots of green fluorescent protein $(GFP)^+$ cells present in MuSC
815 preparations derived from Pax7-nGFP tissue samples using FACS (left) as compared to MACS
816 (right)**. (D)** Enumeration of % total GFP^+ cells enriched from Pax7-nGFP tissue samples using a
817 variety of optimisations that include the number of lineage depletion column rounds with or
818 without an integin-α7 column enrichment round performed during the MACS protocol.
819
820 **Supplementary Figure 4. MACS and FACS sorted MuSCs are functionally similar in mini-**
821 **MEndR assays. (A)** Representative confocal images and **(B)** quantification of yellow fluorescent
822 protein (YFP; yellow) immunostaining coverage of 18M mini-MEndR tissues at 10 DPI that were
823 generated with FACS or MACS sorted MuSCs and treated with DMSO. Scale bar, 500 µm. Graphs
824 display mean ± s.e.m.; unpaired two-tailed T-test with Welch's correction, ns = no significance.
825 n=9-10 tissues from N = 3 independent experiments per cell line.
826
827 **Table 1. Human skeletal muscle myoblast donor information**

828

Age	Sex	Ethnicity	Vendor	Catalog #	Tissue of Origin	Additional Information
18	M	Caucasian	Cook MyoSite	SK-1111-P01236-18M	Rectus Abdominus	Active
18	F	Caucasian	Cook MyoSite	SK-1111-P01431-18F	Vastus Lateralis	Healthy, No known medical conditions
19	F	Caucasian	Cook MyoSite	SK-1111-P01358-19F	Vastus Lateralis	N/A

829

830

831 **Table 2. Culture medium and solutions**

832

Media	Composition
Wash Medium	10 % FBS, 90 % DMEM
Human pMB Growth Medium	Ham's F-10 nutrient mix, 20 % Foetal bovine serum FBS, 5 ng/mL rh-FGF2, 1 % Penicillin-Streptomycin
2D Differentiation Media	DMEM, 2 % Horse serum, 10 g/mL insulin (Sigma, #I6634), 1 % Penicillin-Streptomycin
Rat Tail Collagen Solution	0.1 M Acetic Acid, Collagen I Rat Tail Stock solution (Gibco #A1048301), 0.1 M Acetic Acid, Collagen Stock Solution
MuSC Growth Medium	DMEM/F12, 1 % Pen-strep (P/S), 20 % Foetal bovine serum (FBS), 10 % Horse serum (HS), 1 % 2 mM Q (Glutamax), 1 % Insulin-Transferrin-Selenium (ITS), 1 % Non-Essential Amino acids, 1 % 1 mM Sodium Pyruvate, 50 uM (1/1,000) β-mercaptoethanol, 5 ng/ml (1/5,000) Gibco FGF2
MEndR Growth Medium	Ham's F-10 nutrient mix, 20 % FBS, 1.5 mg/mL 6-Aminocaproic Acid (ACA, Sigma, #A2504), 1 % Penicillin-Streptomycin
MEndR Differentiation Medium	DMEM, 2 % Horse serum, 2 mg/mL ACA, 10 g/mL insulin (Sigma, #I6634), 1 % Penicillin-Streptomycin
Fibrinogen Solution	10 mg/mL Fibrinogen (Sigma, #F8630) in NaCl solution (0.9 % wt/vol in ddH2O)
Extracellular Matrix (ECM) Master Mix	40 % DMEM, 40 % Fibrinogen, 20 % Geltrex™

Red Blood Cell Lysis Buffer	H_2O, 0.155 M NH_4Cl, 0.01 M $KHCO_3$, 0.1 mM EDTA
FACS Buffer	PBS, 2.5 % goat serum, 2 mM EDTA
Blocking Solution	PBS, 10 % goat serum, 0.3 % Triton X-100 (BioShop, #TRX777)

833

834 **Table 3. Antibodies and other reagents**

835

Antibody	Host species	Dilution	Manufacturer
Alexafluor® 647 Anti-Human CD56	Mouse	1:20 (FC)	BD, #557711
eFluor® 660 Anti-Mouse CD34	Rat	1:66 (FC)	eBioscience, #50034182
PE Anti-Mouse α7-Integrin	Rat	1:500 (FC)	AbLab, #530010-05
Biotin Anti-Mouse CD31	Rat	1:200 (FC)	BD, #553371
Biotin Anti-Mouse CD45	Rat	1:500 (FC)	BD, #553078
Biotin Anti-Mouse CD11b	Rat	1:200 (FC)	BD, #553309)
Biotin Anti-Mouse Ly-6A/E	Rat	1:200 (FC)	BD, #553334
Propidium Iodide	-	1:1000	Sigma, # P4864
Anti-Sarcomeric α-actinin	Mouse	1:500	Sigma, #A7811
Anti-GFP	Rabbit	1:500 (IF)	ThermoFisher, #A11122
Anti-Pax7	Mouse	1.5:1 (IF)	Iscove
Alexafluor® 488 Anti-Rabbit	Goat	1:500 (IF)	ThermoFisher, #A11008
Alexafluor® 546 Anti-Mouse	Goat	1:500 (IF)	ThermoFisher, #A11003
Alexafluor® 647 Anti-Rat	Goat	1:500 (IF)	ThermoFisher, #A21247
Phalloidin 568	-	1:500 (IF)	Life Technologies, #A12380

Hoechst	-	1:1000 (IF)	ThermoFisher, #H3570
DRAQ5	-	1:1000 (IF)	Cell Signaling Technology, #4084L
DAPI	-	1:1000 (IF)	Roche, #10236276001
Satellite Cell Isolation Kit	Mouse	1:5 (MACS)	Miltenyi Biotec, #130-104-268
Anti-Integrin-α7 Beads	Mouse	1:5 (MACS)	Miltenyi Biotec, #130-104-261
Click-iT™ Plus EdU Cell Proliferation Kit		(EdU, 1 μM)	ThermoFisher, #C10638

836

837 **Table 4. Small molecule information**

Drug name	Target	Working concentration	Manufacturer
SB203580	p38α/β MAPK	10 μM	New England biolabs, #5633
Erlotinib Hydrochloride	Epidermal Growth Factor Receptor (EGF)	5 μM	Sigma Aldrich, #sc-202154
DMSO	-	-	Sigma Aldrich, #D2650

838

839 **Table 5. Statistical tests and analysis**

Figure	Biological experiments (N)	Total tissues/wells per condition (n)	Total images/wells per tissue	Statistical tests
1C	1 per cell line	3	5	Ordinary one-way ANOVA with Tukey's multiple comparison's test
1D	1 per cell line	3	5	Ordinary one-way ANOVA with Tukey's multiple comparison's test
1E	1 per cell line	3	5	Ordinary one-way ANOVA with

				Tukey's multiple comparison's test
1H	1 per cell line	2	3	Ordinary one-way ANOVA with Tukey's multiple comparison's test
2C	2	8	1	Two-way ANOVA with Sidak's multiple comparisons test
2F	Mixed in: 3 Pre-adsorped: 4	Mixed in: 11 Pre-adsorped:24	1	Unpaired two-tailed t-test
3C	3	Day 7: 9 Day 10: 10 Day 14: 10	1	Ordinary one-way ANOVA with Tukey's multiple comparison's test
3D	3	Day 7: 9 Day 10: 8 Day 14: 6	1	Ordinary one-way ANOVA with Tukey's multiple comparison's test
4C	6	CTX (-): 18 CTX (+): 20	1	Unpaired t-test
4D	5	CTX (-): 15 CTX (+): 16	1	Unpaired t-test
5C	5	DMSO CTX (-):15 DMSO CTX (+):15 p38i CTX (+):15 EGFRi CTX (+):15	1	Ordinary one-way ANOVA with Tukey's multiple comparison's test
5D	4	DMSO CTX (-):12 DMSO CTX (+):12 p38i CTX (+):12 EGFRi CTX (+):10	1	Ordinary one-way ANOVA with Tukey's multiple comparison's test
6C	4	DPI7 DMSO: 11 DPI7 p38i:12 DPI10 DMSO:11 DPI10 p38i:10	1	Multiple t-tests with Welch's correction
6D	3	DPI7 DMSO: 9 DPI7 p38i:9	1	Multiple t-tests with Welch's correction

		DPI10 DMSO:8 DPI10 p38i:9		
7C	3	DMSO: 6 p38i: 8	4-7	Unpaired two-tailed T-test with Welch's correction
7D	3	DMSO: 7 P38i: 8	4-7	Unpaired two-tailed T-test with Welch's correction
7E	3	DMSO: 6 p38i: 8	4-7	Unpaired two-tailed T-test with Welch's correction
7F	3	DMSO: 7 P38i: 8	4-7	Unpaired two-tailed T-test
SI 4B	3	FACS: 9 MACS: 10	1	Unpaired two-tailed T-test with Welch's correction

Figure 1

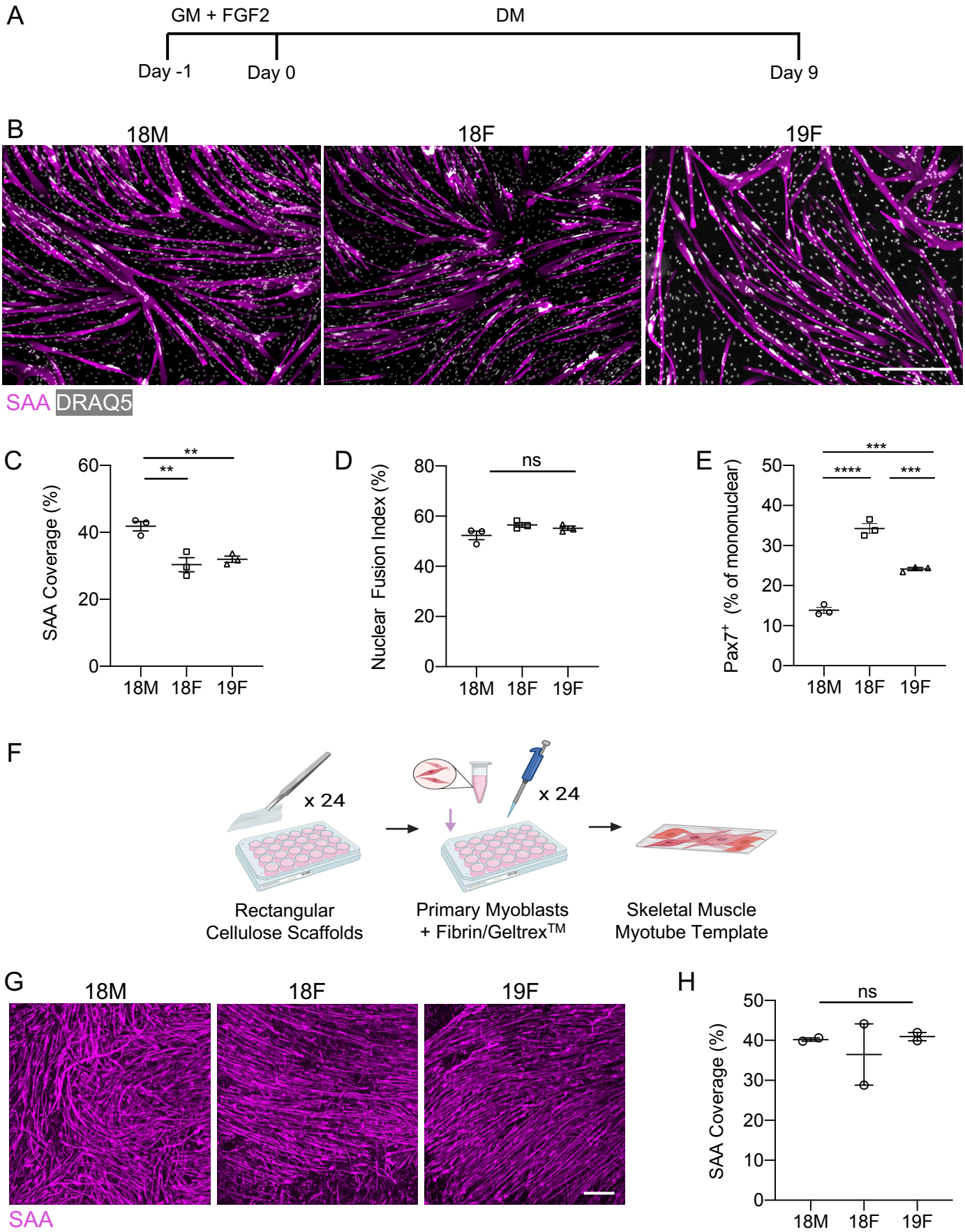
A
GM + FGF2
DM
Day -1
Day 0
Day 9
B
18M
18F
19F
SAA DRAQ5
C
SAA Coverage (%)
60
40
20
0
**
**
18M 18F 19F
D
Nuclear Fusion Index (%)
80
60
40
20
0
ns
18M 18F 19F
E
Pax7+ (% of mononuclear)
50
40
30
20
10
0
***
****
***
18M 18F 19F
F
x 24
x 24
Rectangular Cellulose Scaffolds
Primary Myoblasts + Fibrin/Geltrex™
Skeletal Muscle Myotube Template
G
18M
18F
19F
SAA
H
SAA Coverage (%)
50
40
30
20
10
0
ns
18M 18F 19F

Figure 2

A

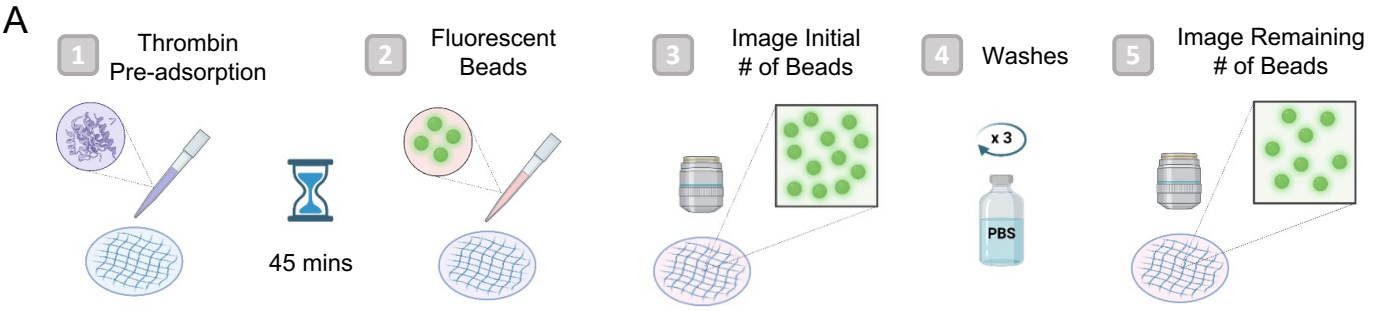

B

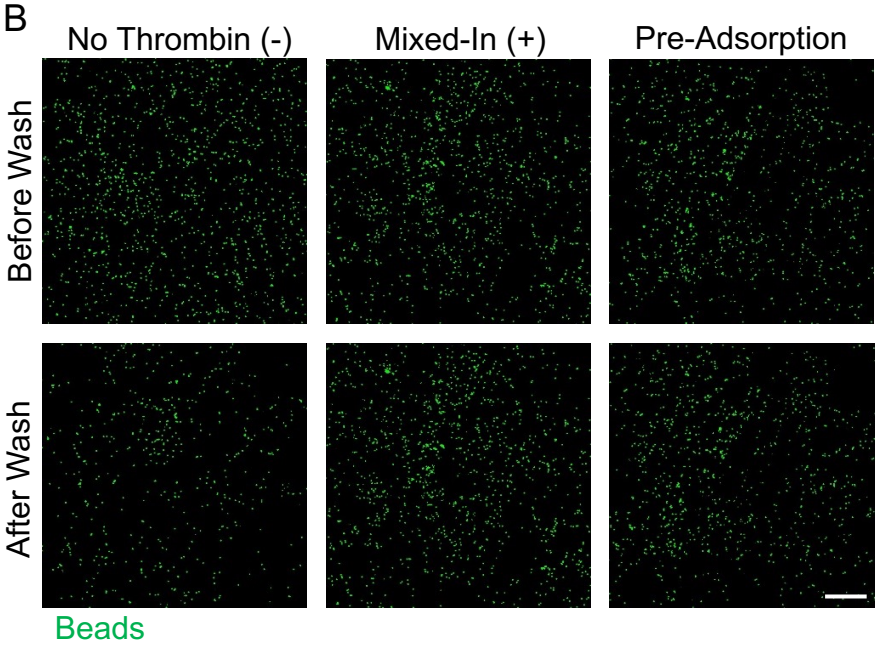

C

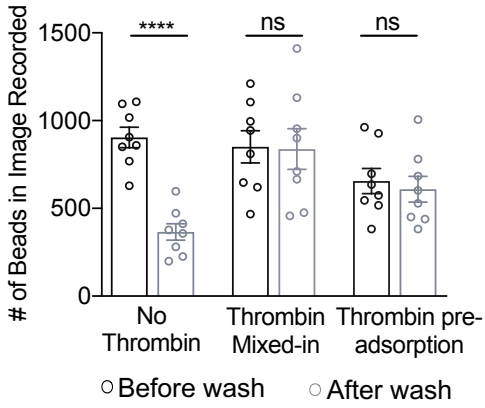

D

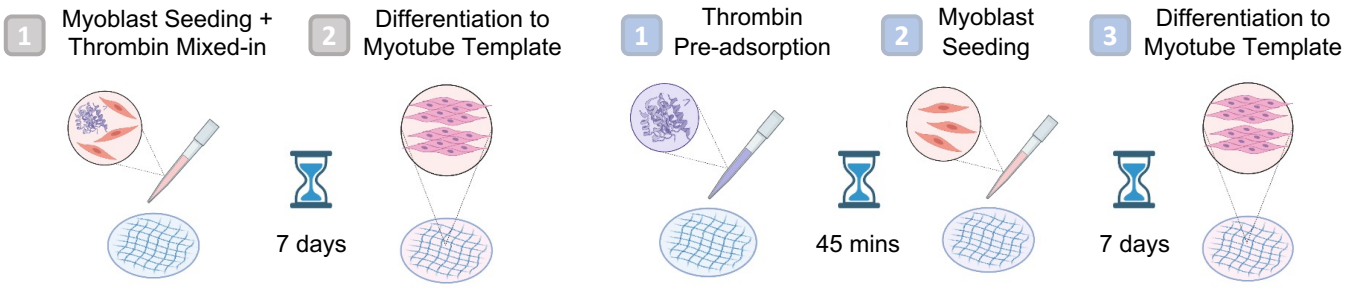

E

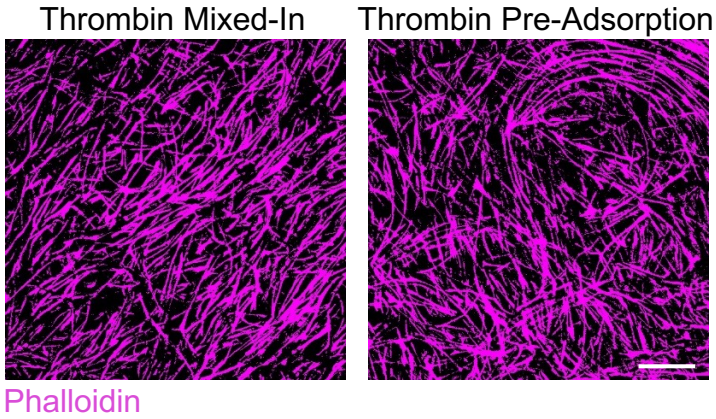

F

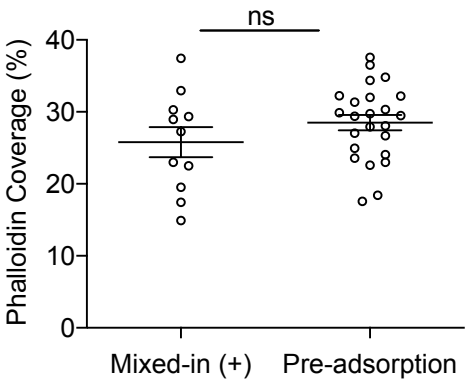

Figure 3

A

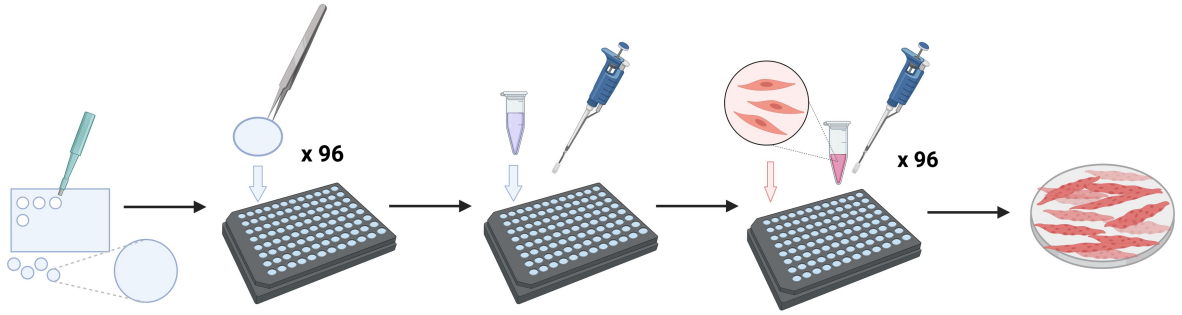

5 mm Circular Cellulose Scaffolds | Scaffolds Placed In Pluronic Coated Wells | Thrombin pre-adsorption | Primary myoblasts mixed in ECM | Mini-Myotube Template

B

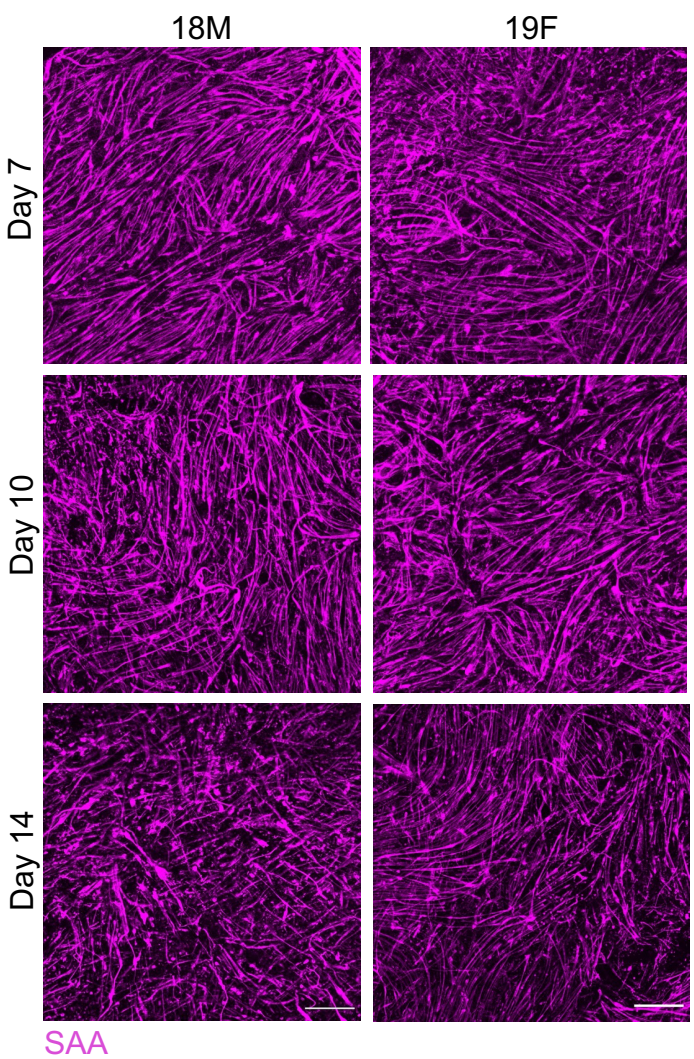

C

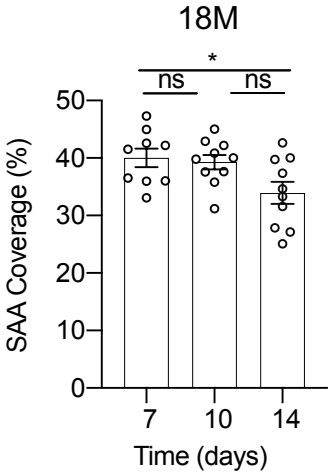

D

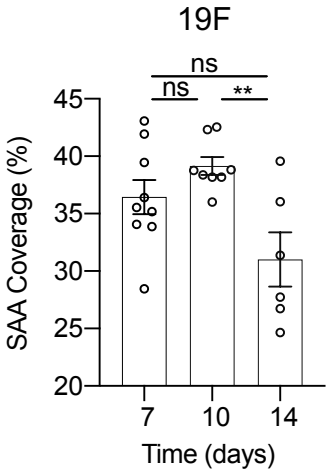

Figure 4

A

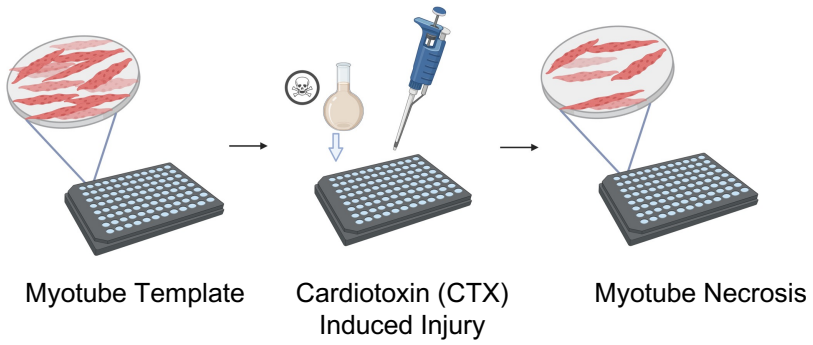

B

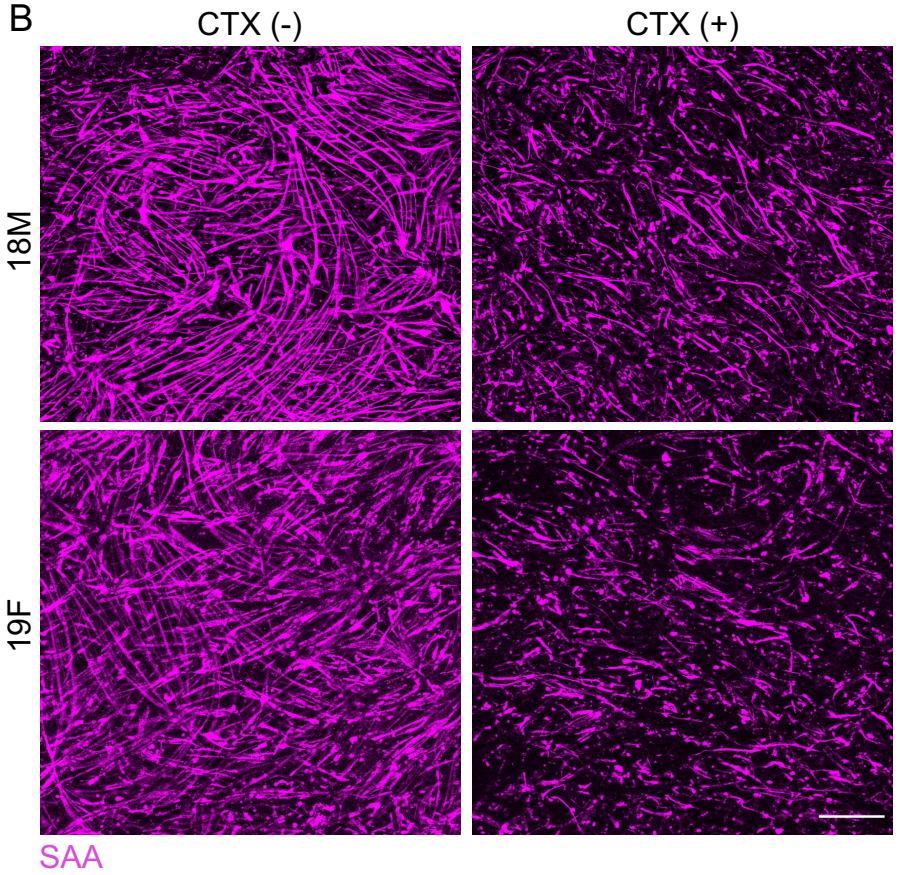

C

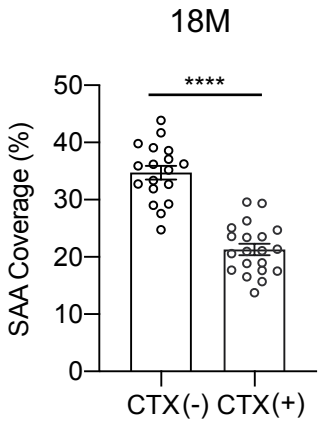

D

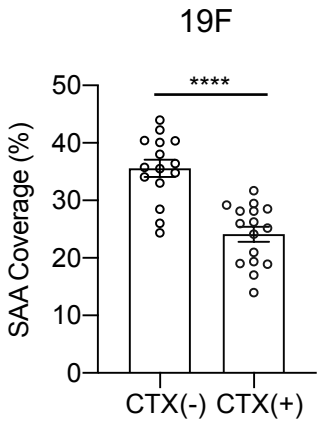

Figure 5

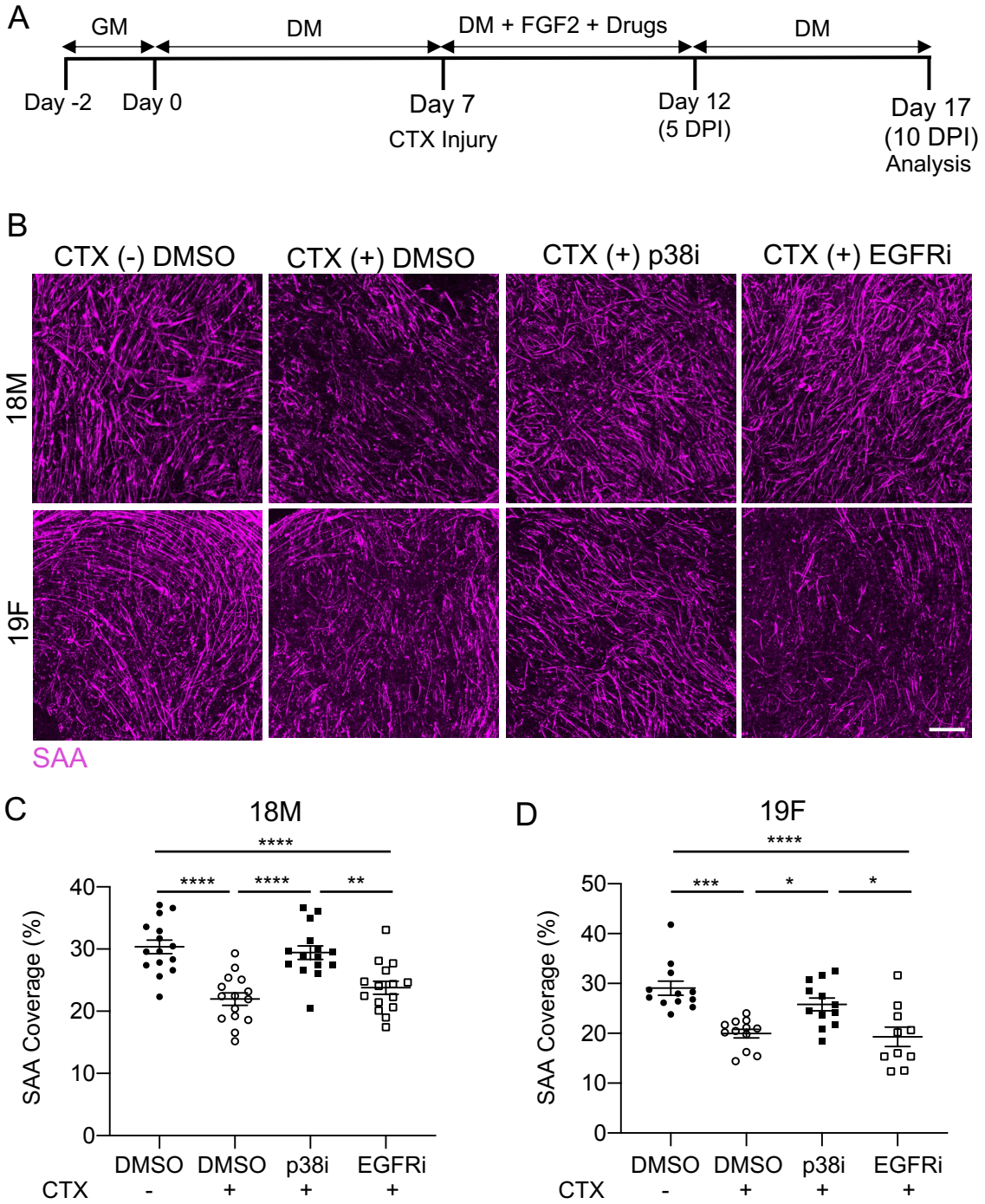
A
GM
DM
DM + FGF2 + Drugs
DM
Day -2
Day 0
Day 7
CTX Injury
Day 12
(5 DPI)
Day 17
(10 DPI)
Analysis
B
CTX (-) DMSO
CTX (+) DMSO
CTX (+) p38i
CTX (+) EGFRi
18M
19F
SAA
C
18M
SAA Coverage (%)
DMSO
DMSO
p38i
EGFRi
CTX
-
+
+
+
D
19F
SAA Coverage (%)
DMSO
DMSO
p38i
EGFRi
CTX
-
+
+
+

Figure 6

A

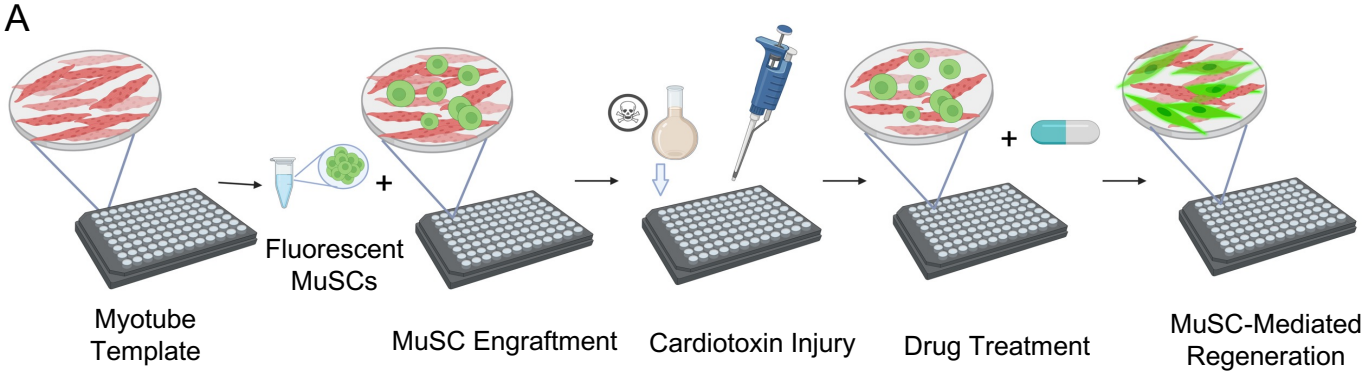

B

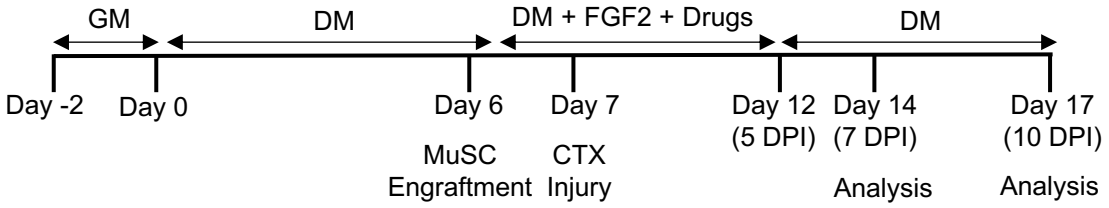

C

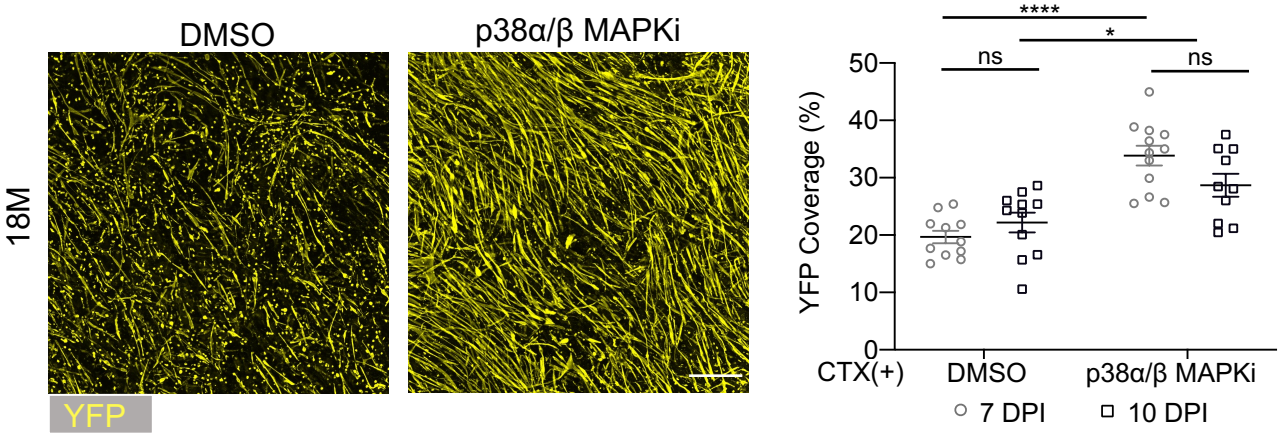

D

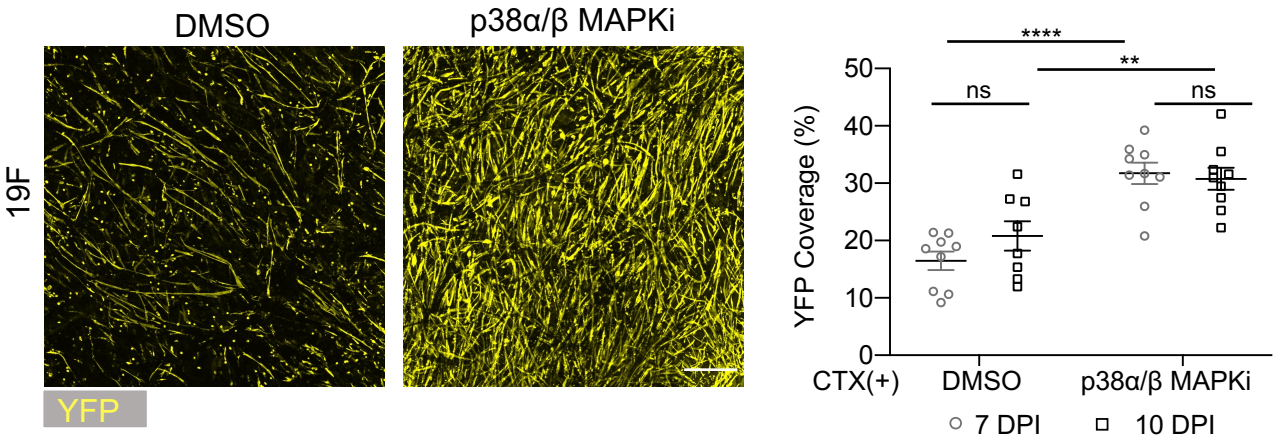

Figure 7

A

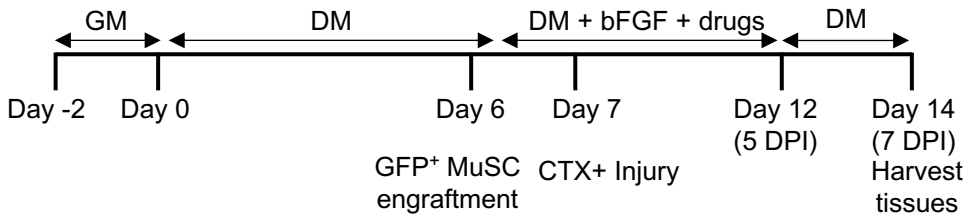

B

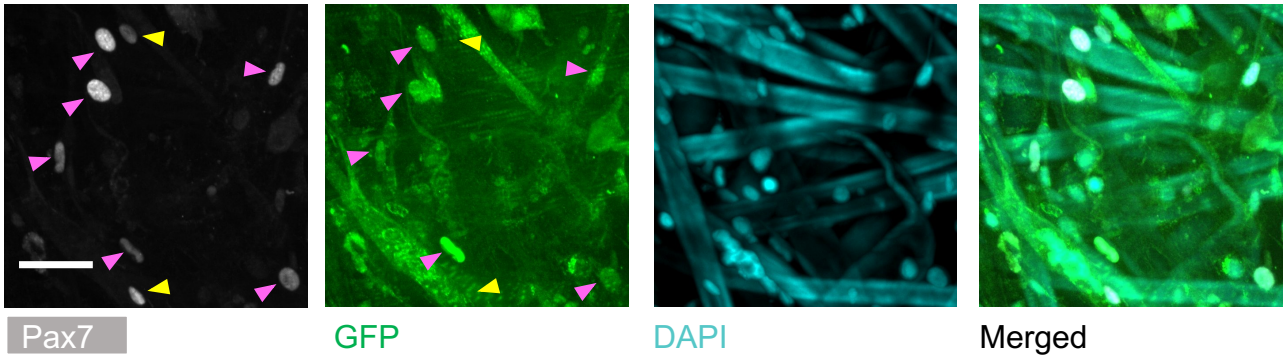

C

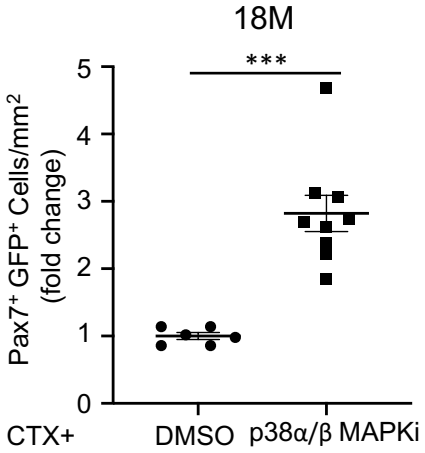

D

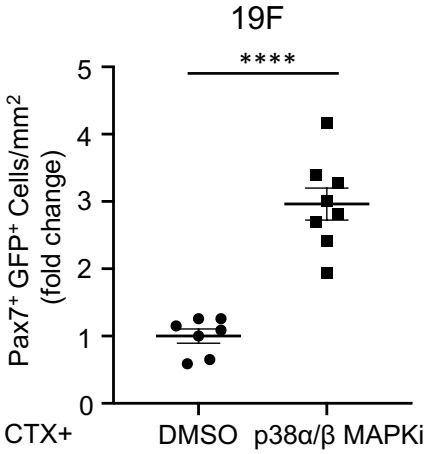

E

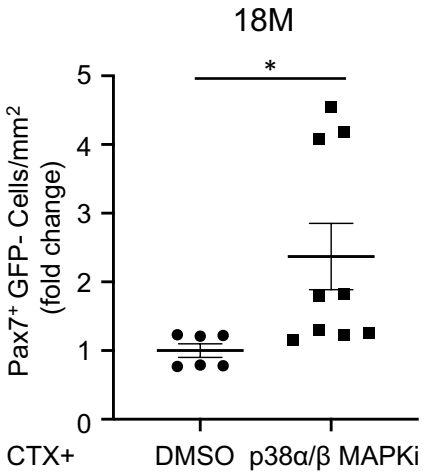

F

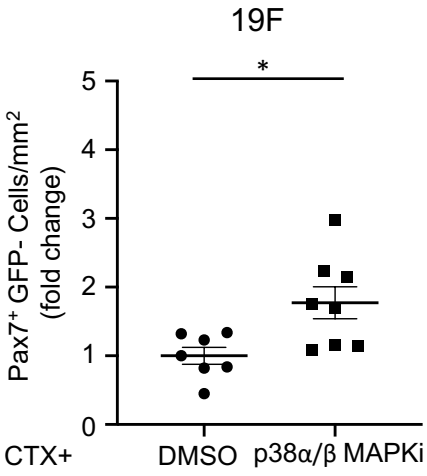

Supplementary Figure 1

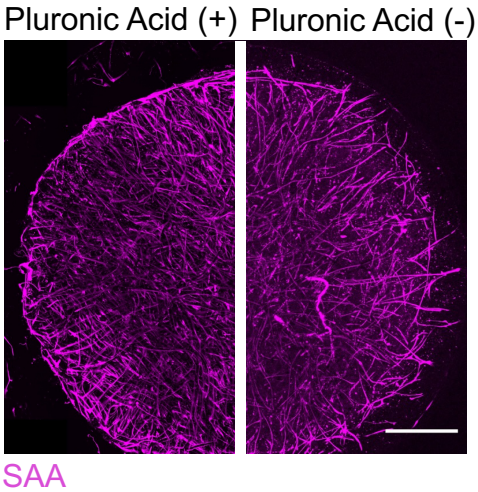

Supplementary Figure 2

A

B

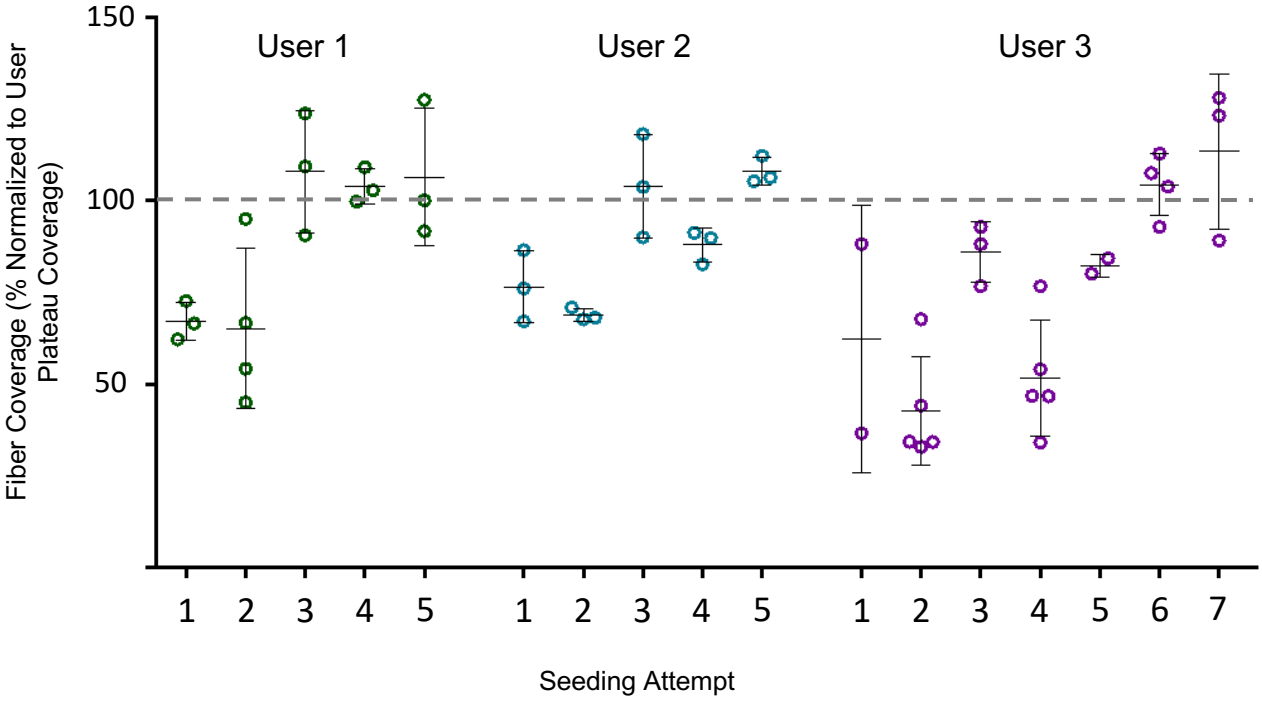

Supplementary Figure 3

A

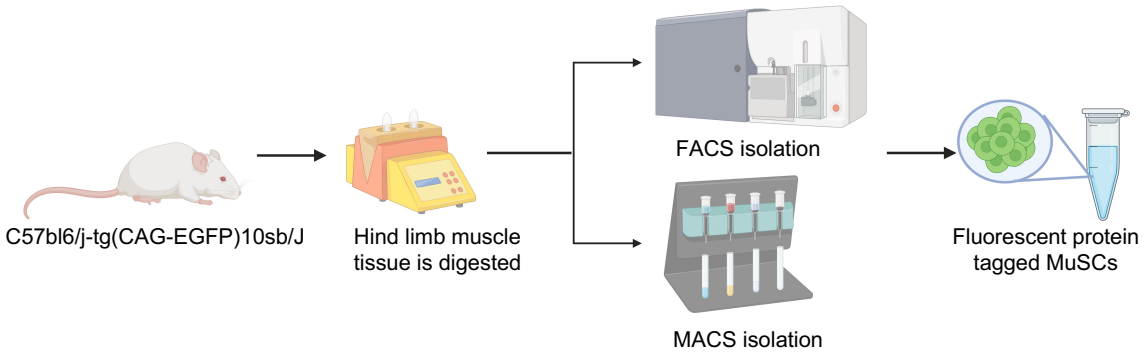

B

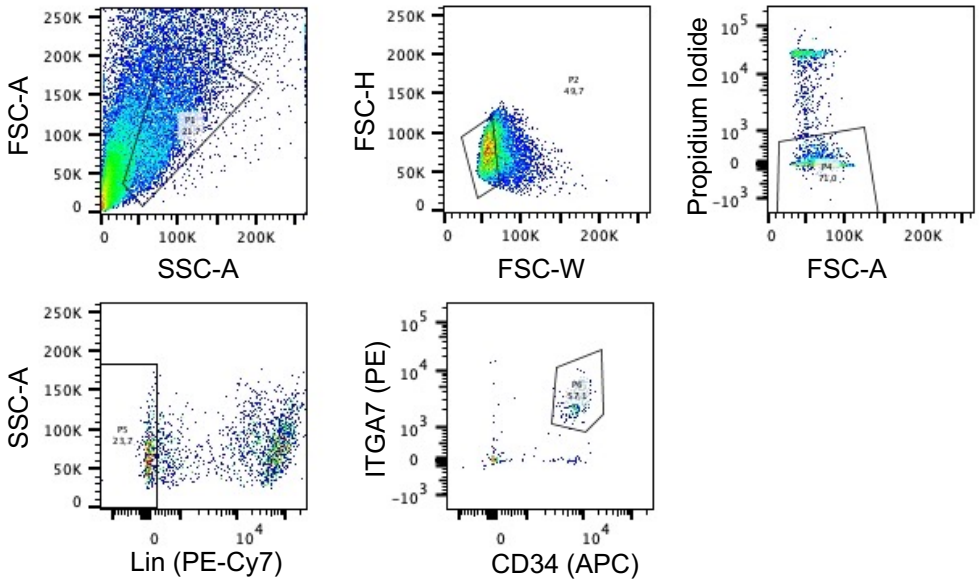

C

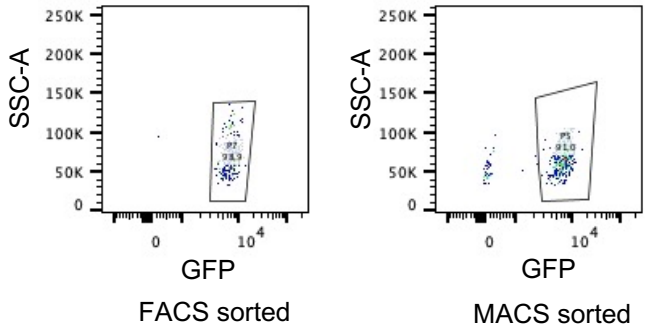

D

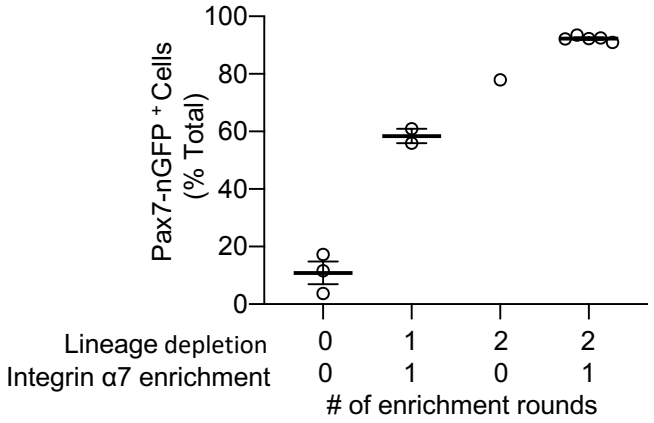
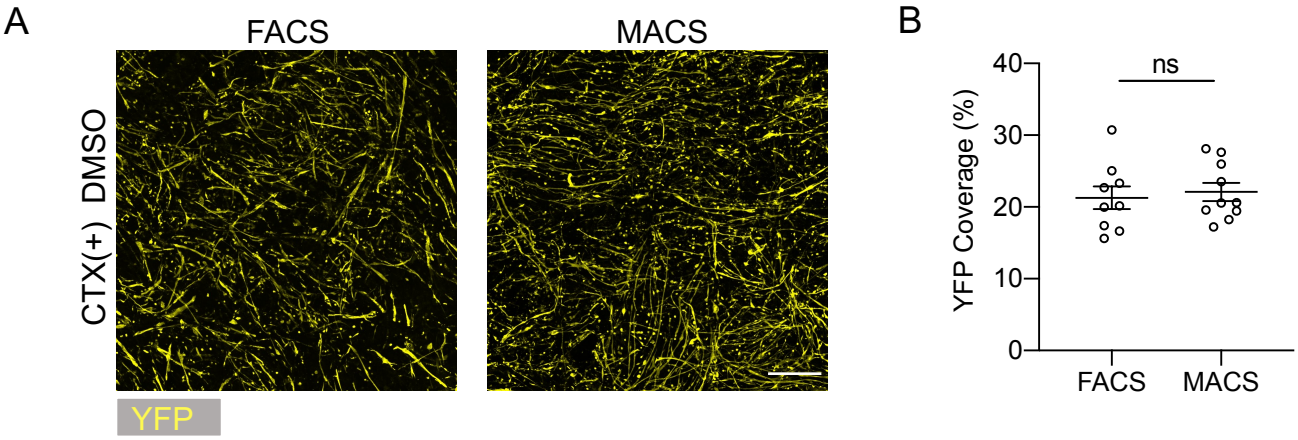
Supplementary Figure 4